

THEORETICAL STUDIES ON ELECTRONIC PROPERTIES OF CURVED
GRAPHENE QUANTUM DOTS AND LITHIUM ADSORPTION ON
GRAPHENE QUANTUM DOTS



Miss Naruwan Pattarapongdilok

จุฬาลงกรณ์มหาวิทยาลัย

บทคัดย่อและแฟ้มข้อมูลฉบับเต็มของวิทยานิพนธ์ตั้งแต่ปีการศึกษา 2554 ที่ให้บริการในคลังปัญญาจุฬาฯ (CUIR)
เป็นแฟ้มข้อมูลของนิสิตเจ้าของวิทยานิพนธ์ ที่ส่งผ่านทางบัณฑิตวิทยาลัย

The abstract and full text of theses from the academic year 2011 in Chulalongkorn University Intellectual Repository (CUIR)
are the thesis authors' files submitted through the University Graduate School.

A Dissertation Submitted in Partial Fulfillment of the Requirements
for the Degree of Doctor of Philosophy Program in Nanoscience and Technology
(Interdisciplinary Program)

Graduate School

Chulalongkorn University

Academic Year 2017

Copyright of Chulalongkorn University

การศึกษาทางทฤษฎีของสมบัติทางอิเล็กทรอนิกส์ของแกรไฟีนควอนตัมดอทชนิดโค้งและการดูดซับ
ลิเทียมบนแกรไฟีนควอนตัมดอท



วิทยานิพนธ์นี้เป็นส่วนหนึ่งของการศึกษาตามหลักสูตรปริญญาวิทยาศาสตรดุษฎีบัณฑิต
สาขาวิชาวิทยาศาสตร์นาโนและเทคโนโลยี (สหสาขาวิชา)
บัณฑิตวิทยาลัย จุฬาลงกรณ์มหาวิทยาลัย
ปีการศึกษา 2560
ลิขสิทธิ์ของจุฬาลงกรณ์มหาวิทยาลัย

Thesis Title THEORETICAL STUDIES ON ELECTRONIC
PROPERTIES OF CURVED GRAPHENE
QUANTUM DOTS AND LITHIUM ADSORPTION
ON GRAPHENE QUANTUM DOTS

By Miss Naruwan Pattarapongdilok

Field of Study Nanoscience and Technology

Thesis Advisor Associate Professor Vudhichai Parasuk, Ph.D.

Accepted by the Graduate School, Chulalongkorn University in Partial
Fulfillment of the Requirements for the Doctoral Degree

..... Dean of the Graduate School
(Associate Professor Thumnoon Nhujak, Ph.D.)

THESIS COMMITTEE

..... Chairman
(Assistant Professor Sukkaneste Tungasmita, Ph.D.)

..... Thesis Advisor
(Associate Professor Vudhichai Parasuk, Ph.D.)

..... Examiner
(Assistant Professor Ratthapol Rangkupan, Ph.D.)

..... Examiner
(Sakulsuk Unarunotai, Ph.D.)

..... Examiner
(Nattapong Paiboonvorachat, D.Phil.)

..... External Examiner
(Chompoonut Rungnim, Ph.D.)

CHULALONGKORN UNIVERSITY

นฤวรรณ ภัทรพงศ์ดีล : การศึกษาทางทฤษฎีของสมบัติทางอิเล็กทรอนิกส์ของแกรฟีนควอนตัมดอทชนิดโค้งและการดูดซับลิเทียมบนแกรฟีนควอนตัมดอท (THEORETICAL STUDIES ON ELECTRONIC PROPERTIES OF CURVED GRAPHENE QUANTUM DOTS AND LITHIUM ADSORPTION ON GRAPHENE QUANTUM DOTS) อ.ที่ปรึกษาวิทยานิพนธ์หลัก: รศ. ดร. วุฒิชัย พาราสุข, 77 หน้า.

แกรฟีนควอนตัมดอท (GQD) ได้รับความสนใจในการประยุกต์ใช้กับอุปกรณ์อิเล็กทรอนิกส์ด้วยสมบัติที่น่าดึงดูดใจ ดังนั้นวิทยานิพนธ์นี้มีจุดมุ่งหมายในการศึกษาสมบัติทางอิเล็กทรอนิกส์ของแกรฟีนควอนตัมดอทชนิดโค้ง (CGQD) และการดูดซับลิเทียมบนแกรฟีนควอนตัมดอท ในการศึกษาแรก แกรฟีนควอนตัมดอทชนิดโค้งถูกสร้างจากแกรฟีนควอนตัมดอทชนิดราบ 2 รูปร่าง ได้แก่ แกรฟีนควอนตัมดอทชนิดสี่เหลี่ยมขนมเปียกปูน และแกรฟีนควอนตัมดอทชนิดหกเหลี่ยม โดยปรับแกนพับและมุมพับต่าง ๆ เสถียรภาพและสมบัติทางอิเล็กทรอนิกส์ของ CGQD ศึกษาด้วยระเบียบวิธี PBE/DNP ผลการศึกษาแสดงให้เห็นว่าพลังงานที่ใช้ในการเปลี่ยนรูปร่างของ GQD ขึ้นกับขนาดและแกนพับไม่ขึ้นกับรูปร่าง การโค้งงอของ GQD ยังทำให้เกิดการเปลี่ยนแปลงของ HOMO-LUMO gap ทั้งที่ทำให้กว้างขึ้นและแคบลง ซึ่งสามารถอธิบายด้วยอันตรกิริยาระหว่างออร์บิทัล ในการศึกษาที่สองได้ศึกษาการดูดซับของลิเทียมไอออนและอะตอมบน GQD 3 ขนาด ได้แก่ โคลโรนิน เซอแคมโคลโรนิน และเซอแคมเซอแคมโคลโรนิน ที่ตำแหน่งต่าง ๆ ของ GQD ตำแหน่งดูดซับและพลังงานยึดเหนี่ยวหาด้วยระเบียบวิธี M06-2X/6-31g(d) ผลการศึกษาระบุว่า ลิเทียมไอออนและอะตอมสามารถยึดจับได้ดีกว่าที่บริเวณขอบของ GQD โดยการดูดซับระหว่างลิเทียมไอออนและโคลโรนินมีการยึดจับมากที่สุดเท่ากับ -135.073 กิโลแคลอรีต่อโมล ยิ่งไปกว่านั้น การเพิ่มขนาดของ GQD เพิ่มพลังงานการยึดจับ ยกเว้นการดูดซับลิเทียมไอออนบน GQD ประจุ -1 ตำแหน่งการดูดซับของลิเทียมไอออนและอะตอมบน GQD สามารถอธิบายด้วยประจุรวมของวง 6 เหลี่ยม นอกจากนี้ ความสามารถในการยึดจับของระบบลิเทียม 1 ไอออนบน GQD มากกว่าระบบลิเทียม 2 ไอออน สำหรับระบบลิเทียม 2 ไอออนยังขึ้นกับการผลัดกันระหว่างลิเทียมไอออน

สาขาวิชา วิทยาศาสตร์นาโนและเทคโนโลยี

ปีการศึกษา 2560

ลายมือชื่อนิติดี

ลายมือชื่อ อ.ที่ปรึกษาหลัก

5587851020 : MAJOR NANOSCIENCE AND TECHNOLOGY

KEYWORDS: ELECTRONIC STRUCTURE / CURVED GRAPHENE / QUANTUM DOTS
/ HOMO-LUMO GAP / LITHIUM / ADSORPTION

NARUWAN PATTARAPONGDILOK: THEORETICAL STUDIES ON
ELECTRONIC PROPERTIES OF CURVED GRAPHENE QUANTUM DOTS
AND LITHIUM ADSORPTION ON GRAPHENE QUANTUM DOTS.
ADVISOR: ASSOC. PROF. VUDHICHAH PARASUK, Ph.D., 77 pp.

Graphene quantum dots (GQDs), with their attractive properties, are of interest to apply for electronic devices. Therefore, this dissertation aimed to investigate the electronic of curved graphene quantum dots (CGQDs) and the adsorption of lithium on GQDs. For the first part, two shapes of flat GQDs, rhomboidal (RGQDs) and hexagonal (HGQDs), were modified to make CGQDs with different folding axes and angles. Stabilities and electronic properties of CGQDs were studied using PBE/DNP. The results showed that the deformation energies of GQDs depend on sizes and folding axes but not their shapes. HOMO-LUMO gap variations, both widening and narrowing the gap, upon folding were observed, and can be explained by orbital interactions. In the second study, three sizes of GQDs, coronene, circumcoronene, and circumcircumcoronene were allowed to be adsorbed by lithium ions and atoms at various positions of GQDs. Adsorption positions and binding energies were determined using M06-2X/6-31g(d). The results indicated that lithium ion and atom could bind better at the edge of GQDs. The adsorption between lithium ion and coronene showed the highest binding affinity of -135.073 kcal/mol. Moreover, the size increment of GQDs raises the binding energy, except Li^+ adsorption on GQDs with -1 charge. Preferred adsorption positions of lithium ions and atoms on GQDs can be described by the total charge of six-membered ring. In addition, binding affinities of one-Li-ion system on GQDs are larger than two-Li-ion system. For two Li-ion system, the binding energy on GQDs also depends on Li ion-Li ion repulsion.

Field of Study: Nanoscience and Technology Student's Signature

Academic Year: 2017

Advisor's Signature

ACKNOWLEDGEMENTS

My utmost gratitude goes to my thesis advisor, Assoc. Prof. Dr. Vudhichai Parasuk. During the time, he gave me suggestions about several things such as physical chemistry theories, computational methods, journal and thesis writing, and the “theory of life”, and he has been a good master teacher for me with responsibility, punctuality, empathy, and academic expertise.

I would like to acknowledge all committee members for my doctoral dissertation, Asst. Prof. Dr. Sukkaneste Tungasmita, Asst. Prof. Dr. Rattapol Rangkupan, Dr. Sakulsuk Unarunotai, Dr. Nattapong Paiboonvorachat, and Dr. Chompoonut Rungnim who gave me suggestions during examination.

I would like to thank all members of Computational Chemistry Unit Cell for their companionship and friendship.

I would like to acknowledge the financial supports provided by Center of Innovative Nanotechnology (CIN), Chulalongkorn University and Bansomdejchao-praya Rajabhat University. Moreover, the support of computer resources and other facilities by the computer science program at Bansomdejchaopraya Rajabhat University and the Center of Excellence in Computational Chemistry of Chulalongkorn University must be as well acknowledged.

Finally, I am forever indebted to my parents and family members for their encouragement and understanding throughout the entire study.

CONTENTS

	Page
THAI ABSTRACT	iv
ENGLISH ABSTRACT.....	v
ACKNOWLEDGEMENTS.....	vi
CONTENTS.....	vii
LIST OF FIGURES	viii
LIST OF TABLES	x
CHAPTER I INTRODUCTION.....	1
CHAPTER II THEORETICAL BACKGROUND.....	9
2.1 Density functional theory	9
2.2 Electrochemistry of Lithium ion batteries	11
CHAPTER III COMPUTATIONAL DETAILS	12
3.1 Electronic properties of curved graphene quantum dots	12
3.2 Adsorptions of lithium atom/ion on graphene quantum dots	14
CHAPTER IV RESULTS AND DISCUSSION.....	18
4.1 Electronic properties of curved graphene quantum dots	18
4.2 Adsorptions of lithium atom/ion on graphene quantum dots	37
CHAPTER V CONCLUSIONS	43
REFERENCES	45
APPENDIX.....	52
VITA.....	77

LIST OF FIGURES

		Page
Figure 1.1	Mother of all graphitic forms. Graphene is a 2D building material for carbon materials of all other dimensionalities. It can be wrapped up into 0D buckyballs, rolled into 1D nanotubes or stacked into 3D graphite.	1
Figure 1.2	Energy gap –size relation for GQDs.....	2
Figure 1.3	Schematic diagram of the top-down and bottom-up methods for synthesizing GQDs.	3
Figure 1.4	Comparison of the different battery technologies in terms of volumetric and gravimetric energy density.	4
Figure 1.5	Illustration of the components in a lithium ion cell.....	5
Figure 1.6	Illustrations of layered, spinel, and olivine structures which are materials use for positive electrode LIB; (a) LiCoO ₂ layered structure, (b) LiMn ₂ O ₄ spinel structure, (c) LiFePO ₄ olivine structure.	6
Figure 1.7	Structures of (a) coronene C ₂₄ H ₁₂ , (b) circumcoronene C ₅₄ H ₁₈ , and (c) circumcircumcoronene C ₉₆ H ₂₄	8
Figure 2.1	A schematic presentation of the most commonly used Li-ion battery based on graphite anodes and LiCoO ₂ cathodes.....	11
Figure 3.1	(a) Rhomboidal-shape GQDs and (b) Hexagonal-shape GQDs.....	12
Figure 3.2	Distinct folding axes of (a) RGQDs and (b) HGQDs.....	13
Figure 3.3	Adsorption positions on the hexagonal unit.	15
Figure 3.4	Lithium positions on three GQDs; (a) coronene, (b) circumcoronene, and (c) circumcircumcoronene.	16
Figure 4.1	HOMO-LUMO gap as the function of folding angles; (a) a2x2 structures, (b) a3x3 structures, (c) a4x4 structures, (d) a5x5 structures, and (e) a6x6 structures	20
Figure 4.2	Relation between folding angle and average sp ² angle; (a) rhomboidal-shape CGQDs of a4x4 and (b) hexagonal-shape CGQDs of b4x4.....	21
Figure 4.3	Comparison of HOMO and LUMO energies at 2 and 16 degrees of (a) a3x3FA1, (b) a3x3FA2, (c) a3x3FA3, and (d) a3x3FA4.....	24

Figure 4.4	Illustrations of HOMO and LUMO orbitals of a3x3; (a) FA1, (b) FA2, (c) FA3, and (d) FA4	25
Figure 4.5	Side view structures of a6x6 at the folding angle of 14 degree when folded along (a) FA2 and (b) FA3.	26
Figure 4.6	HOMO-LUMO gap change with folding angles; (a) b2x2 structures, (b) b3x3 structures, (c) b4x4 structures, (d) b5x5 structures, and (e) b6x6 structures.....	29
Figure 4.7	Comparison of HOMO and LUMO energies at 12 and 14 degrees of (a) b3x3FA1 and (b) b3x3FA2	30
Figure 4.8	Comparison of HOMO and LUMO of b3x3; (a) FA1 and (b) FA2	31
Figure 4.9	Deformation energies for different folding axes of RGQDs at various folding angles; (a) a2x2 structures, (b) a3x3 structures, (c) a4x4 structures, (d) a5x5 structures, and (e) a6x6 structures	33
Figure 4.10	Deformation energies for different folding axes of HGQDs at various folding angles; (a) b2x2 structures, (b) b3x3 structures, (c) b4x4 structures, (d) b5x5 structures, and (e) b6x6 structures.....	35
Figure 4.11	Relation between deformation energies at 16° and numbers of carbon atoms for FA2 of RGQDs, FA3 of RGQDs, FA2 of HGQDs, FA1 of RGQDs, FA4 of RGQDs, and FA1 of HGQDs.....	36
Figure 4.12	Lithium positions on three GQDs; (a) C ₂₄ H ₁₂ , (b) C ₅₄ H ₁₈ , and (c) C ₉₆ H ₂₄	37
Figure 4.13	Relation between 1/R and adsorption energies of GQD-2Li ⁺ complexes	40

LIST OF TABLES

	Page
Table 3.1 Charges and spin multiplicities of GQDs and GQD-Li/Li ⁺ complexes.....	15
Table 3.2 Charges and spin multiplicities of lithium atom and ion.	15
Table 3.3 Adsorption patterns of two Li-ion on C ₂₄ H ₁₂ and C ₅₄ H ₁₈	17
Table 4.1 Average sp ² angle of rhomboidal-shape CGQDs.....	22
Table 4.2 Average sp ² angle of hexagonal-shape CGQDs.....	27
Table 4.3 Adsorption energies in kcal/mol of one Li ion on GQDs with negative (q = -1), neutral (q = 0), and positive (q=1) charge at various adsorbed sites.....	37
Table 4.4 Net charges of lithium ion, C ₆ ring of GQD, and total GQD.....	38
Table 4.5 Adsorption energies per ion of two Li-ion on C ₂₄ H ₁₂ and C ₅₄ H ₁₈ with various charges.....	39
Table 4.6 Adsorption energies of Li atom on C ₂₄ H ₁₂ , C ₅₄ H ₁₈ , and C ₉₆ H ₂₄ with q = -1, q=0, and q = 1.....	41
Table 4.7 Net charges of lithium atom and C ₆ of Li-GQD complexes	42
Table S1 HOMO-LUMO gaps of CGQDs.....	53
Table S2 Charges of lithium ions of GQDs-2Li ⁺ complexes	60
Table S3 Average charges of GQDs and Li ⁺ of GQDs-2Li ⁺ complexes.....	61
Table S4 Positions of two lithium ion on negative charged GQD	62
Table S5 Positions of two lithium ion on neutral GQD	67
Table S6 Positions of two lithium ion on positive charged GQD	72

CHAPTER I

INTRODUCTION

Nowadays, electronic devices play important roles in our daily life. Nanomaterials are being of interest, since they can be used for improving the performance of the devices. A particular nanomaterial which has outstanding properties is graphene.

Graphene has hexagonal network (honeycomb lattice) and is a two-dimensional (2D) single layer of sp^2 -hybridized carbons. It is the initial building block of well-known materials such as graphite (3D), nanotubes (1D), and fullerenes (0D) [1-5] (Figure 1.1). Graphene has remarkable properties such as 1-atom thickness, excellent transmittance and conductivity, ultra high stiffness, strong elasticity, and high thermal stability [6-7].

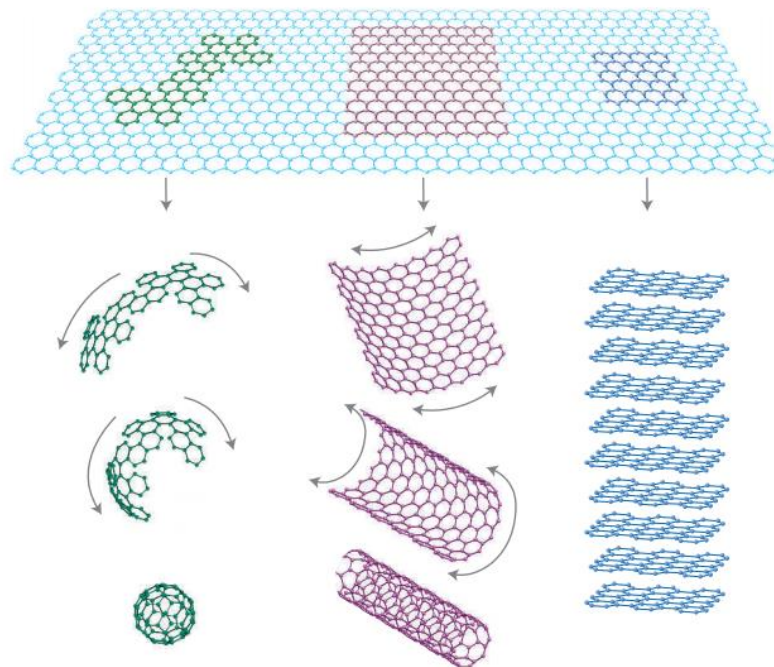


Figure 1.1 Mother of all graphitic forms. Graphene is a 2D building material for carbon materials of all other dimensionalities. It can be wrapped up into 0D buckyballs, rolled into 1D nanotubes or stacked into 3D graphite.

Reprinted with permission from ref [6]. Copyright 2007, Springer Nature.

When graphene contains one to ten layers and have the dimensions in the range of a few nm to ~ 100 nm, typically below 20 nm, it can be named “Graphene quantum dots (GQDs)” [8-9]. The GQD has distinguished properties such as high specific surface area, high electron mobility, eco-friendly, strong luminescence, good hole transport ability, high solubility in various solvents, low toxicity, etc. in which they are used for the bio-sensing, display, and energy applications [8, 10-15].

Ritter *et. al.* [16] performed an experimental study and has shown that the energy band gap of both zigzag-edge and armchair-edge GQDs decreases when the size of GQD increases. (Figure 1.2). There have been many theoretical works [17-19] on edge and size effects of GQDs that support the finding of Ritter *et. al.* Consequently, modifying its size, edge, surface, and geometry can control the band gap of GQDs [8, 13, 16, 20] which leads to required conductivity.

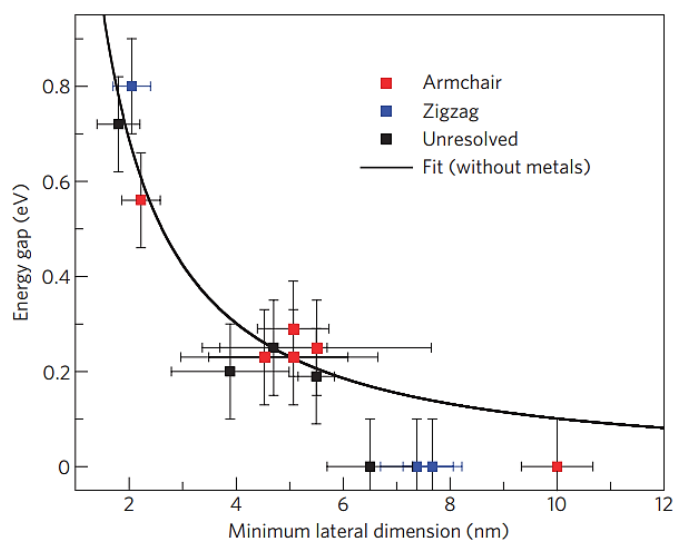


Figure 1.2 Energy gap –size relation for GQDs.

Reprinted with permission from ref [16]. Copyright 2009, Springer Nature.

GQDs can be prepared from two main processes, top-down and bottom-up approaches (see Figure 1.3). For the top-down method, GQD is created from the decomposition and exfoliation of bulk graphene-based materials such as graphite. This method requires concentrated acids, strong oxidizing agents, and high temperatures [21-26]. In bottom-up method, GQD is synthesized from aromatic molecules such as fullerenes. This approach needs complicated reaction steps and

special organic reagents. Furthermore, the size and properties of final products can be controlled by this method [21-26].

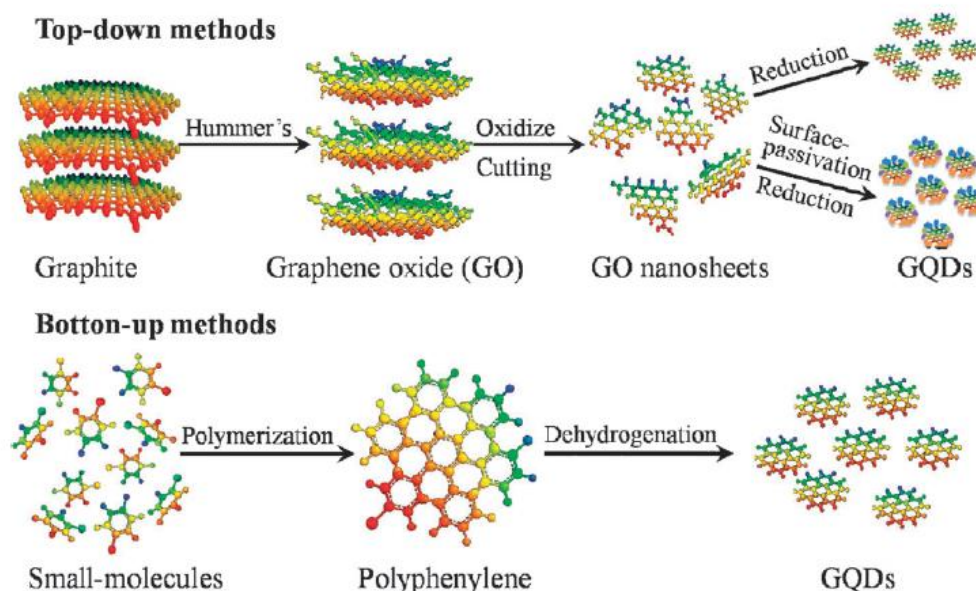


Figure 1.3 Schematic diagram of the top-down and bottom-up methods for synthesizing GQDs.

Reprinted with permission from ref [13]. Copyright 2012, Royal Society of Chemistry.

GQDs or rather flat GQDs can be transformed to curved GQDs (CGQDs) by applying force to their structures. This often happens when one wants to apply the material for making electronic devices. Electronic properties of CGQDs are therefore of interest. However, there has been very little numbers of studies on electronic properties of CGQDs. There were a few studies concerning curved graphene nanoribbons. Graphene nanoribbons (GNRs) are the strip of graphene with the length of > 10 and the width of < 50 nm [27]. It was reported that the band gap energy of curved GNRs depended on the curvature, in which the reduction in the band gap energy with enhanced curvature was observed [28]. Furthermore, longer GNRs have lower strain energy than the shorter one [29].

Today energy technologies shift the production of electricity from using burning fuel to sustainable energy sources, such as wind and solar energies, which unfortunately fluctuate during the day. Hence, technologies for energy storage especially batteries are required. Lithium-ion or Li-ion battery (LIBs) is currently one of the most popular rechargeable batteries. Additionally, LIBs is commonly used in home electronics especially for electronic devices such as mobile phones, digital cameras, computer notebooks, etc. [30]. This is because LIBs have high energy and high power density, long lifetime, and environmentally friendly [31]. Figure 1.4 shows the different battery technologies in terms of volumetric density are compared with in gravimetric energy density.

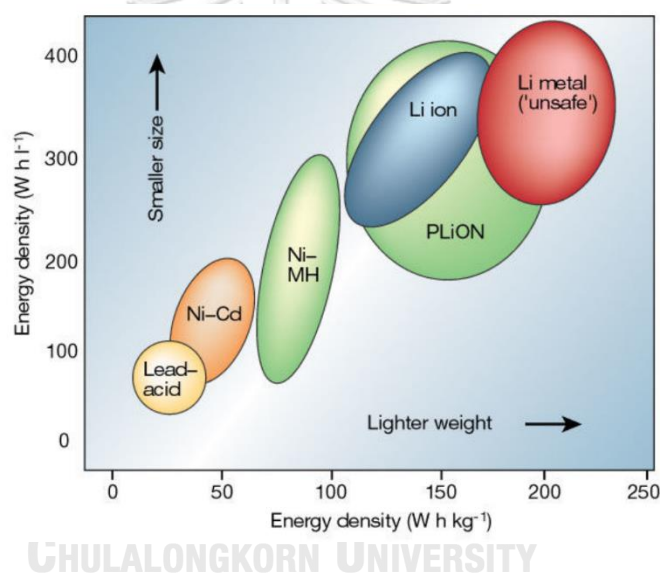


Figure 1.4 Comparison of the different battery technologies in terms of volumetric and gravimetric energy density.

Reprinted with permission from ref [32], Copyright 2001, Springer Nature.

Potential advantages of LIBs are high energy-/power-density, rechargability, flexible and thin design, and longer lifetime [33-35]. For these reasons, LIBs have been used in electric vehicles and smart electronic storage [32]. The experiments concerning lithium batteries began in 1912 by American chemist G.N. Lewis but the first rechargeable lithium battery was invented in 1976 by British chemist M.S. Whittingham [36]. Titanium (IV) sulfide and lithium metal were used as the

electrodes. Nevertheless, the titanium disulfide was an unsuitable selection because it is an expensive material and very difficult to synthesize.

Generally, LIB consists of three primary functional components which are positive charged electrode (cathode), negative charged electrode (anode) and conducting electrolyte [37] (Figure 1.5). Between cathode and anode, there is a membrane made of polypropylene/polyethylene, for separating and preventing the electrical contact. Moreover, the membrane allows lithium-ion to diffuse from the electrodes during the process of charging and discharging [38].

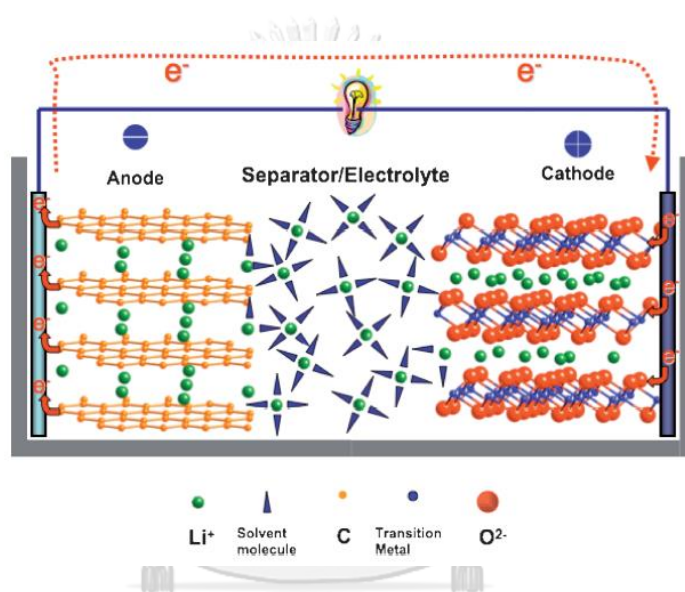


Figure 1.5 Illustration of the components in a lithium ion cell.

Reprinted with permission from ref [39]. Copyright 2009, Royal Society of Chemistry.

The first use of lithium-ion battery in commercial was initiated by Sony Corporation which is consisted of lithium-cobalt-oxide (LiCoO_2) as cathode and graphite as anode. This type of LIBs still is used in most electronic devices. In the commercially popular lithium-ion battery, the cathode is mostly made from materials with three different structures which are a layered oxide (e.g. LiCoO_2 , LiNiO_2), a spinel (e.g. LiMnO_4), and an olivine (e.g. LiMnPO_4 , LiFePO_4). Figure 1.6 shows the structure of each cathode material. The cathode with the layered structure, LiCoO_2 , is mostly used in portable devices because it has the highest energy density. Nevertheless, the cobalt element is very expensive and environmental hazard. The spinel structure, LiMn_2O_4 , is cheaper and eco-friendly but unstable in high

temperature environment (more than 50°C). The olivine structure, LiFePO_4 , has low conductivity but is currently interested in the battery industry due to its low production costs, superior recyclability and stability at high temperature. The LiFePO_4 has already been employed in many commercial batteries especially in electric vehicles (EV).

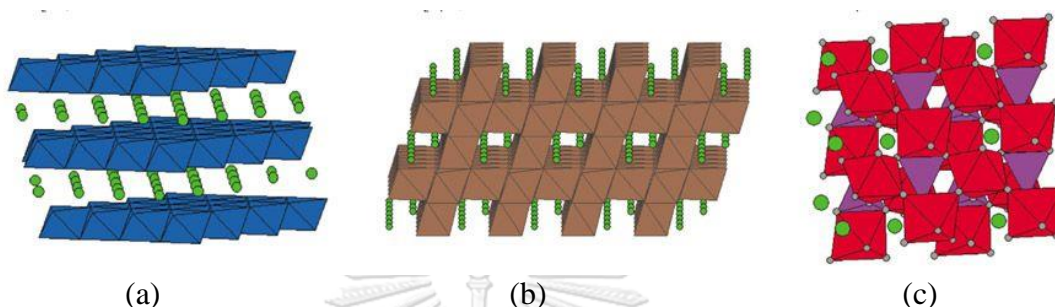


Figure 1.6 Illustrations of layered, spinel, and olivine structures which are materials use for positive electrode LIB; (a) LiCoO_2 layered structure, (b) LiMn_2O_4 spinel structure, (c) LiFePO_4 olivine structure.

Reprinted with permission from ref [40]. Copyright 2002, Springer Nature.

It was found that the graphite intercalation compounds [41] and nano-carbonaceous materials [42] are greatly effective for the anode. The most negative electrode of lithium-ion rechargeable batteries is based on the nano-carbonaceous PAS (polyacenic semiconductive) discovered by Tokio Yamabe [43]. Graphite is commonly used for the anode of LIB due to its high conductivity since it has delocalized π -electrons and appropriate structure for lithium ion intercalation and diffusion [44]. However, only six carbon atoms (C_6) of graphite are allowed to be intercalated by one Li ion, stoichiometrically LiC_6 , and results in low power density [38]. Hence, there are many researches that studied both carbon and non-carbon materials for higher performance and capacity of the anode. The examples anode materials are carbon nanotubes, carbon nanofibers, titanium, silicon, and graphene.

There are two types of lithium-ion battery electrolytes, i.e. liquid and solid electrolyte. The liquid electrolytes contain varying ratio of lithium salts (i.e. LiPF_6 , LiBF_4 and LiClO_4) in alkyl organic carbonates such as ethylene carbonates, propylene carbonates, dimethyl carbonates. For batteries, the solid electrolytes are safer than

liquid electrolytes because it has no leaks. The solid electrolytes of batteries uses lithium metal oxides which is ceramic. The lithium ion can fast transport through it.

Previous studies supported that small sheets of carbon such as graphite materials and amorphous carbon materials has higher efficiency than that the crystalline graphite [45-46] owing to the size effect. It improves the performance of lithium-ion batteries by quick absorption, short diffusion lengths, and fast diffusion rates [47]. Thus, the reduction of Li^+ becomes faster and hence it gives high power density and a quick charge. GQDs which have small size can be used to enhance efficiency of LIBs. There are applications where GQDs being composite component or coated material in LIBs [11, 48]. The behavior of Li/Li^+ adsorption over GQDs is of interest. Umadevi and Sastry found that the interaction energy between Li/Li^+ and neutral graphene at the edge is higher than at the center of $\text{C}_{24}\text{H}_{12}$ hexagonal-shaped GQD or coronene [49]. When larger GQD such as circumcircumcoronene ($\text{C}_{96}\text{H}_{24}$ hexagonal-shape GQD) was studied, it was found that the charge of carbon atoms at the edges was more negative and lithium ion at the edges was smaller positive than at the center position [50]. Sadlej-Sosnowska calculated interaction energies between three GQDs (coronene, circumcoronene, circumcircumcoronene, Figure 1.7) and lithium atom and they discovered that the interaction energy is diminished with the increasing size of GQDs [51]. Recently, Novák calculated the binding energies of lithium ion on coronene and coronene derivatives in external electric field [52]. This model mimics the condition in the battery. The strong binding energies between Li^+ and coronene of -45.5 kcal/mol was obtained [52].

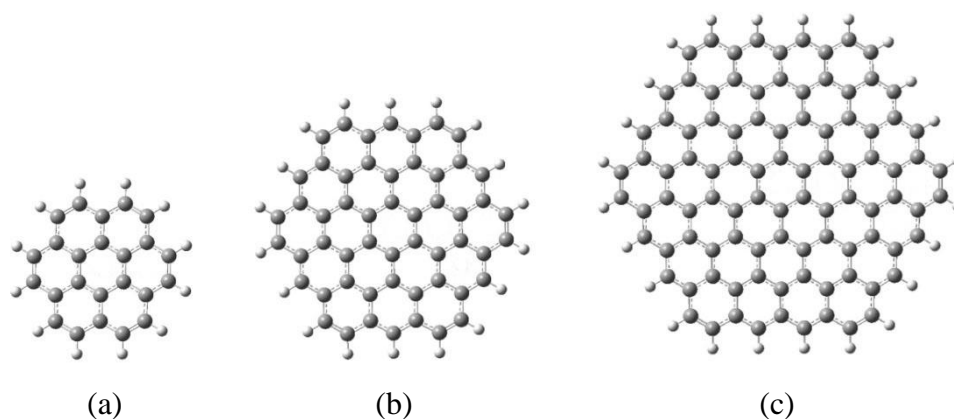


Figure 1.7 Structures of (a) coronene $C_{24}H_{12}$,
(b) circumcoronene $C_{54}H_{18}$, and (c) circumcircumcoronene $C_{96}H_{24}$

In the first part of our study, we are interested in electronic properties of CGQDs at various sizes, shapes, folding axes, and folding angles. Additionally, we are also interested in how easy CGQDs can be formed. For scope of this work, two kinds of curved graphene quantum dots (hexagonal and rhomboidal shapes) with different curvature will be built and calculated using Density Functional Theory (DFT). Electronics and mechanical properties of curved graphene quantum dots (CGQDs) will be monitored. The understanding on electronic and mechanical properties of CGQDs can be applied for the design GQDs-based electronic devices. In the second part, adsorptions of lithium ion(s)/atom on several sizes of charged and uncharged hexagonal GQDs were studied using DFT. We would like to gain the understanding of the adsorption of Li/Li^+ on GQDs. We hope that this knowledge will lead to the better design of LIBs.

CHAPTER II

THEORETICAL BACKGROUND

2.1 Density functional theory

In Density Functional Theory (DFT) [53], the electronic energy as the functional of the density $E[\rho]$ is given by

$$E[\rho] = T_s[\rho] + v_{ext}[\rho] + J[\rho] + E_{xc}[\rho] \quad (2.1)$$

where $T_s[\rho]$ is the kinetic energy of the system of non-interacting particles, $v_{ext}[\rho]$ is the external potential or the interaction of electron-nuclear, $J[\rho]$ is the classical Coulombic interaction,

and

$$E_{xc}[\rho] = (T[\rho] - T_s[\rho]) + (V_{ee}[\rho] - J[\rho])$$

$T[\rho]$ is the total kinetic energy and $V_{ee}[\rho]$ is the electron-electron repulsion interaction. The last term in Eq. (2.1) includes the contribution of exchange and correlation energies.

According to Kohn-Sham [54], the charge density can be constructed from

$$\rho(r) = \sum_i |\phi_i(r)|^2 \quad (2.2)$$

where the sum is total occupied KSOs (Kohn-Sham orbitals alias Molecular orbitals), ϕ_i .

The molecular orbitals (MOs) can possibly be occupied by either spin-up (alpha) or spin-down (beta) electron. The use of the similar ϕ_i for both of them is called as the *spin-restricted* calculation. The use of dissimilar ϕ_i is accepted as a calculation of the *spin-unrestriction* or the *spin-polarization*. In the unrestricted situation, it is probable that densities of two different charge, alpha MOs and beta MOs, are generated. Their summation gives the total charge density, while their difference gives the *spin density* that is the quantity of excess alpha over beta spin.

This is similar to Hartree-Fock calculations for restriction and unrestriction wave function (Pople and Nesbet) [55].

We cannot find the exact description for the last term in Eq. (2.1) which is the energy of exchange-correlation functional. The estimation is therefore needed. The local density approximation (LDA) which models using the uniform electron gas (Hedin and Lundqvist [56]; Ceperley and Alder [57]; Lundqvist and March [58]) is the simplest approximation and yields reasonable results. This approximation is on the basis that the charge density changes quite slowly (i.e., each of molecular region surely seems a uniform electron gas). Thus, the energy of exchange-correlation functional is given by

$$E_{xc}[\rho] \cong \int \rho(r) \varepsilon_{xc}[\rho(r)] dr \quad (2.3)$$

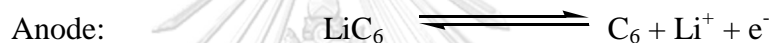
where $\varepsilon_{xc}[\rho]$ is the exchange-correlation per particle in a uniform electron gas. Slater (1951) simply used $\varepsilon_{xc}[\rho] = \rho^{1/3}$ to derive the simplest form of the exchange-correlation potential. However, the correlation is not included in this approximation. So, the Slater term is dubbed as “exchange” only. Moreover, to add the electron correlation more sophisticated approximations, as derived by Vosko, Wilk, and Nusair (VWN) [59], Von Barth and Hedin (BH) [60], Janak, Moruzzi, and Williams (JMW) [61], and Perdew and Wang (PW) [62], can be included.

The later step in development of the local density (LDA) model is taking into account the inhomogeneity that has occurring in any molecular system. This is helping by incorporating with the density gradient expansion. This approach is named “Generalized Gradient Approximation” (GGA). It is also called “non-local” density approximation. Generally, the use of GGA functionals includes the correlation functional by Perdew and Wang (PW91), and the gradient-corrected exchange functional by Becke (B) or BPW91, or the Becke functional and the gradient-corrected correlation functional by Lee, Yang, and Parr (LYP) or BLYP. Modern DFT parametrically incorporates the “exact” or “hartree-fock” exchange to the functional, named “hybrid” functional. Examples of hybrid DFTs are B3LYP, B3PW91, M06-2X [63], etc. These hybrid functionals have been shown to improve calculation results immensely.

2.2 Electrochemistry of Lithium ion batteries

The operation of lithium-ion battery involves the movement of lithium ion between the electrodes through the electrolyte and separator. Both cathode and anode allow Li ions to move in, called intercalation, and move out, called deintercalation, of their structures. During charging, the positive lithium ions (Li^+) move from the cathode to the anode through the electrolyte and intercalate into the graphite structure, at the same time, the electrons (e^-) also move along the external circuit in the same direction. During discharging, the reverse process occurs. The example of chemical reactions that takes place LIB using LiCoO_2 as cathode and graphite as anode are as follows.

Discharging condition:



The full reaction of charging (left to right) and discharging (right to left) are as follows.



The basic reaction processes are illustrated in Figure 2.1.

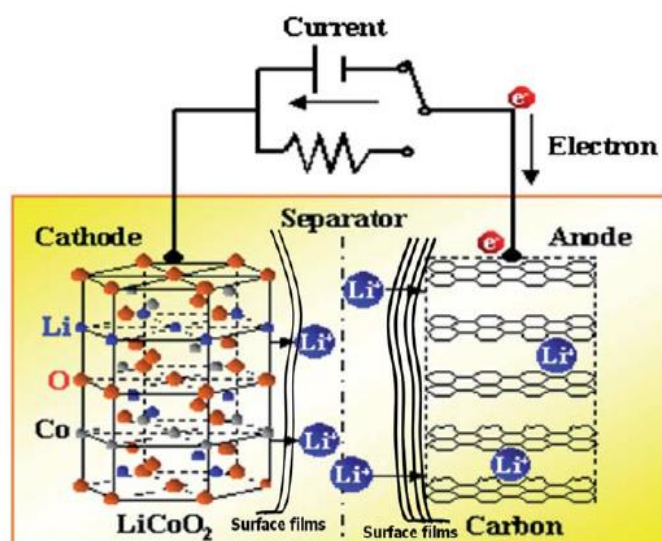


Figure 2.1 A schematic presentation of the most commonly used Li-ion battery based on graphite anodes and LiCoO_2 cathodes.

Reprinted with permission from ref [64]. Copyright 2011, Royal Society of Chemistry.

CHAPTER III

COMPUTATIONAL DETAILS

Electronic properties of curved graphene quantum dots and lithium atom/ion adsorption on graphene quantum dots were investigated using Density Functional Theory. Details of calculations were given in this chapter.

3.1 Electronic properties of curved graphene quantum dots

3.1.1 Electronic properties

Two structural analogs of GQDs consisting of rhomboidal graphene quantum dots (RGQDs) and hexagonal graphene quantum dots (HGQDs) shapes as shown in Figure 3.1 were studied.

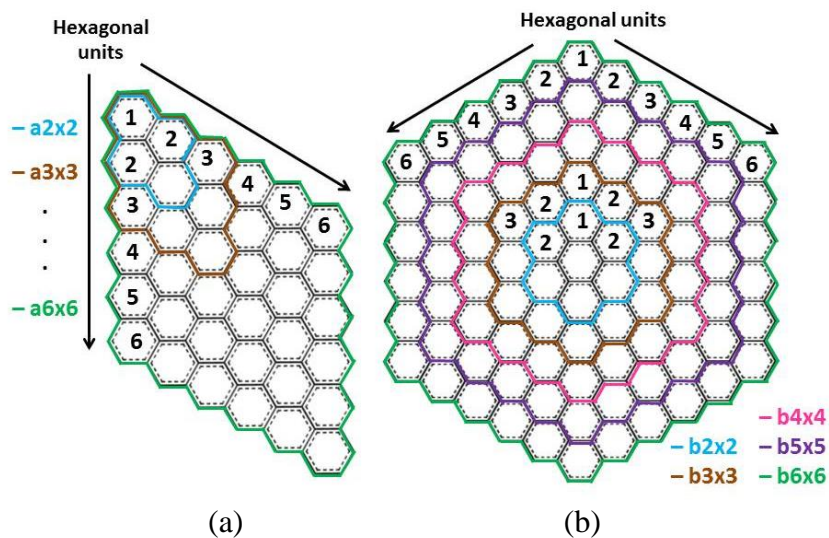


Figure 3.1 (a) Rhomboidal-shape GQDs and (b) Hexagonal-shape GQDs.

Both structural analogs were obtained from a single layer of graphite taken from the library of the Material Studio 5.5 program [65]. Models of RGQDs are represented by “ $an \times n$ ” reflecting $n \times n$ hexagonal units where $n = 2 - 6$. All terminal C atoms were saturated by H atom giving $C_{16}H_{10}$ ($a2 \times 2$), $C_{30}H_{14}$ ($a3 \times 3$), $C_{48}H_{18}$ ($a4 \times 4$), $C_{70}H_{22}$ ($a5 \times 5$), and $C_{96}H_{26}$ ($a6 \times 6$), Figure 4.1 (a). Since the hexagonal-shape contains three $n \times n$ rhombic structures, models of HGQDs are then denoted by “ $bn \times n$ ” for $n =$

2 – 6. Similar to RGQDs terminal carbons of HGQDs were capped by H atoms. Thus, they consist of $C_{24}H_{12}$ (b2x2), $C_{54}H_{18}$ (b3x3), $C_{96}H_{24}$ (b4x4), $C_{150}H_{30}$ (b5x5), and $C_{216}H_{36}$ (b6x6), Figure 3.1 (b). All GQDs were fully optimized using DFT with Perdew, Burke, and Ernzerhof (PBE) [66] functional and double numerical plus polarization (DNP) [67-68] basis set of DMol3 program in Material Studio 5.5 suite, which has been tested that can calculate the energies and structures nearly experiments and have high speed calculation for graphene. Finally, optimized GQDs were folded or curved along “symmetry-unique” axes at the incremental of 2° to 16° to create CGQDs using Visual Molecular Dynamics (VMD) program.

For RGQDS, there are four symmetry-unique folding axes, FA1, FA2, FA3, and FA4, Figure 3.2a., whereas there are only two symmetry-unique folding axes, FA1 and FA2 for HGQDs (Figure 3.2b).

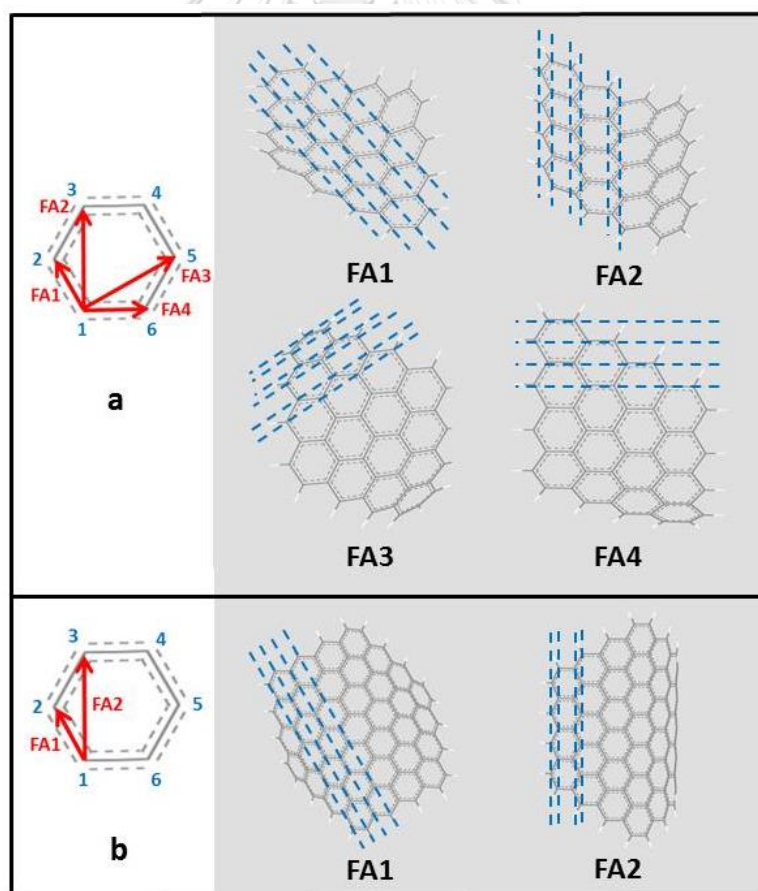


Figure 3.2 Distinct folding axes of (a) RGQDs and (b) HGQDs.

From Figure 3.2, we noticed that the folding along FA1 and FA4 of RGQDs and FA1 of HGQDs is through “zigzag” carbon atoms. Thus, the folding along those axes is named “zigzag-like folding”. While the folding along FA2 and FA3 of RGQDs and FA2 of HGQDs is through “armchair” carbons and the name “armchair-like” folding is given. These notations is in line with Casabianca et.al. [69]. For a particular symmetry-unique folding axis and GQD structure (size and shape), there are more than one axis of that type. For example, a2x2 RGQD ($C_{16}H_{10}$) has 9 FA1, 12 FA2, 16 FA3, and 10 FA4 axes, while b4x4 HGQD ($C_{96}H_{24}$) has 15 and 16 FA1 and FA2 axes, respectively. All symmetry-unique axes were folded simultaneously at the designated degree. For CGQDs, only positions of hydrogen atoms were optimized at the same level of theory. Energies and HOMO/LUMO energies of GQDs and CGQDs were obtained at this level of theory and their optimized geometries.

3.1.2 Deformation energies

Deformation energies of CGQDs were calculated from the difference between the total energy of CGQD and total energy of flat GQD following Eq. (3.1):

$$\text{Deformation energy} = E_{\text{CGQD}} - E_{\text{GQD}} \quad (3.1)$$

where E_{CGQD} = energy of CGQD,

E_{GQD} = energy of flat GQD

3.2 Adsorptions of lithium atom/ion on graphene quantum dots

For the study of lithium atom/ion adsorptions on GQDs, three sizes of hexagonal-shape GQDs, b2x2 (coronene $C_{24}H_{12}$), b3x3 (circumcoronene $C_{54}H_{12}$), and b4x4 (circumcircumcoronene $C_{96}H_{24}$), were used. In addition, Li/Li⁺ adsorptions were performed on GQDs with 0 (neutral), +1, and -1 molecular charge. The three charges were set to represent different conditions of GQDs (GQDs will be used as electrodes in Li-ion battery). The positive/negative charge of GQDs denotes discharging/charging condition of the battery. All geometry optimizations were accomplished at the M06-2X/6-31G(d) level of theory [63], one of the best functionals for the study of noncovalent interactions, without any constraints using the

Gaussian 09 package [70]. Additionally, lithium ion or lithium atom was adsorbed at hollow position above hexagonal unit of GQDs (Figure 3.3). This setup is in line with experimental evidences, in which LiC_6 was found to be stoichiometric number of Li^+ /graphite intercalation. [38].

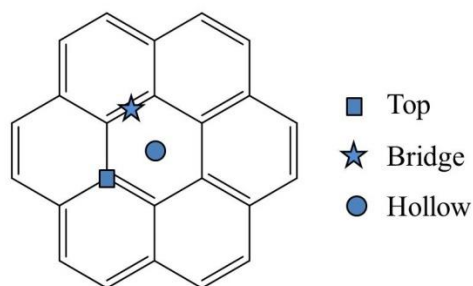


Figure 3.3 Adsorption positions on the hexagonal unit.

Total charges and spin multiplicities of GQDs, GQD-Li/Li^+ , and GQD-2Li^+ complexes were set according to Table 3.1, while the total charge and spin multiplicity of lithium atom/ion were given in Table 3.2.

Table 3.1 Charges and spin multiplicities of GQDs and GQD-Li/Li^+ complexes.

GQDs		GQD - Li Complex		GQD - Li^+ Complex		GQD - 2Li^+ Complex	
Charges	$2S+1$	Charges	$2S+1$	Charges	$2S+1$	Charges	$2S+1$
-1	2	-1	3	0	2	1	2
0	1	0	2	1	1	2	1
1	2	1	3	2	2	3	2

Table 3.2 Charges and spin multiplicities of lithium atom and ion.

Types	Charges	$2S+1$
Li atom	0	2
Li ion	1	1

For one-Li-atom/ion system, possible adsorption positions of Li/Li⁺ over three sizes of GQDs were studied and the positions are shown in Figure 3.4. While the adsorbed positions for two-Li-ion system were displayed in Figure 3.5. The adsorption energy (ΔE_{ad}) or the binding affinity of Li/Li⁺ over GQDs were obtained by the following equation:

$$\Delta E_{ad} = E_{GQD-X} - (E_{GQD} + E_X) \quad (3.2)$$

where E_{GQD-X} = energy of GQD-Li/Li⁺ complex,

E_{GQD} = energy of GQD

E_X = energy of dopant (Li/Li⁺).

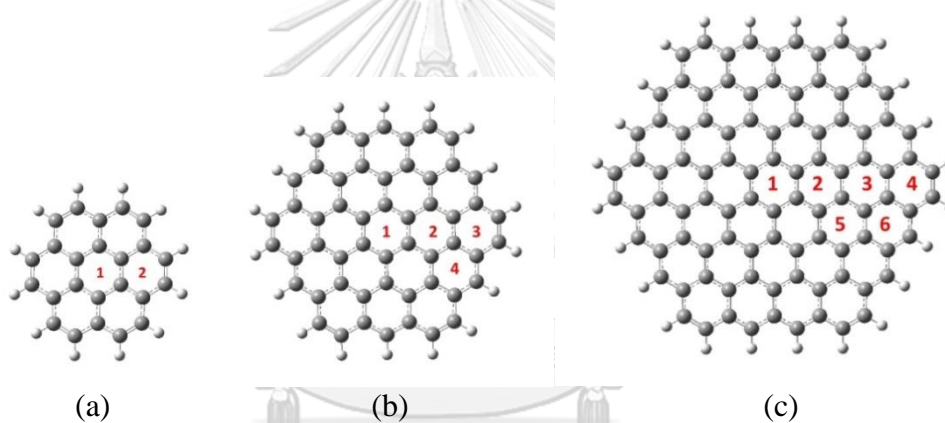
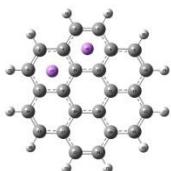
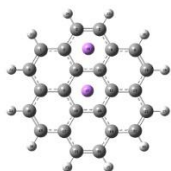

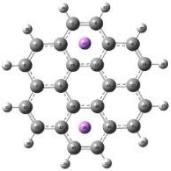
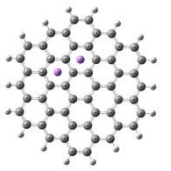
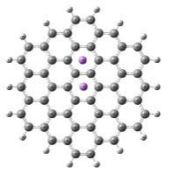
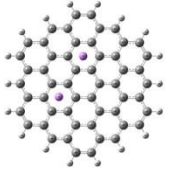
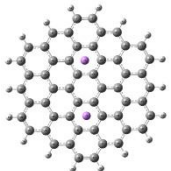
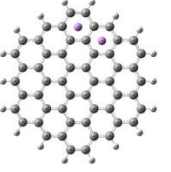
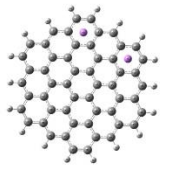
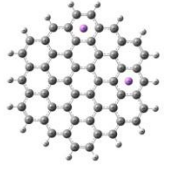
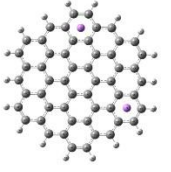
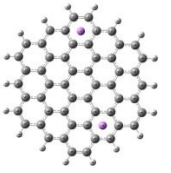
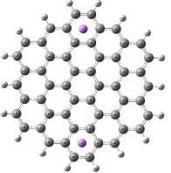
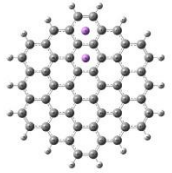
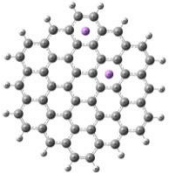
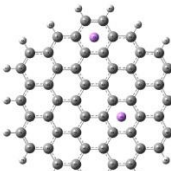
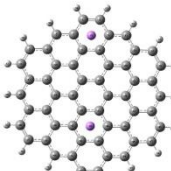
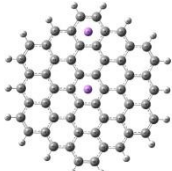


Figure 3.4 Lithium positions on three GQDs; (a) coronene, (b) circumcoronene, and (c) circumcircumcoronene.

Table 3.3 Adsorption patterns of two Li-ion on $C_{24}H_{12}$ and $C_{54}H_{18}$

$C_{24}H_{12}$	Pattern 1	Pattern 2	Pattern 3	Pattern 4
				
	Pattern 1	Pattern 2	Pattern 3	Pattern 4
				
Pattern 5	Pattern 6	Pattern 7	Pattern 8	
$C_{54}H_{18}$				
	Pattern 9	Pattern 10	Pattern 11	Pattern 12
				
	Pattern 13	Pattern 14	Pattern 15	
				

CHAPTER IV

RESULTS AND DISCUSSION

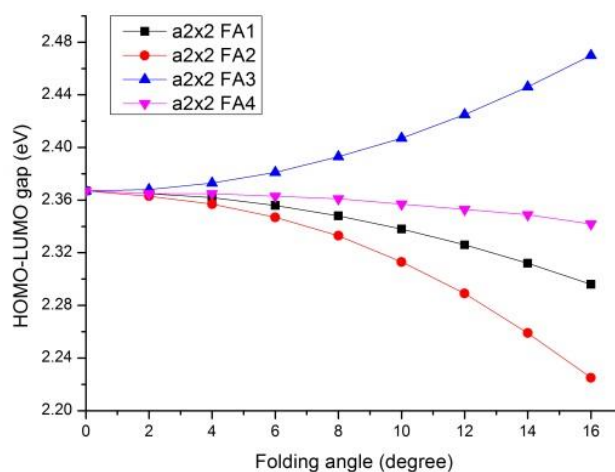
This chapter is divided into two parts; electronic properties of CGQDs, and adsorption of Li/Li⁺ on GQDs.

4.1 Electronic properties of curved graphene quantum dots

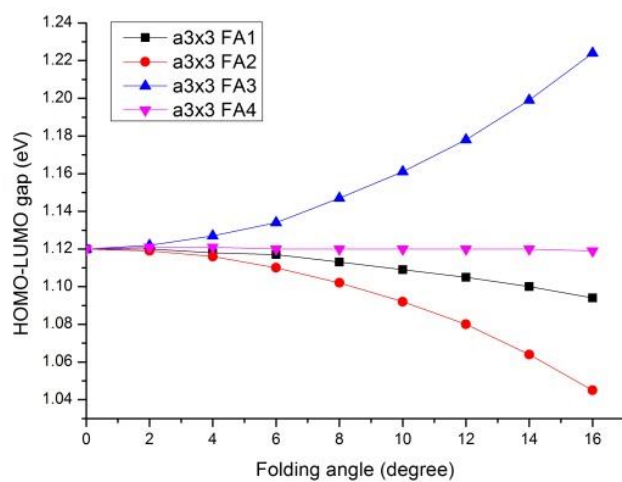
4.1.1 Electronic properties

4.1.1.1 Rhomboidal-shape CGQDs

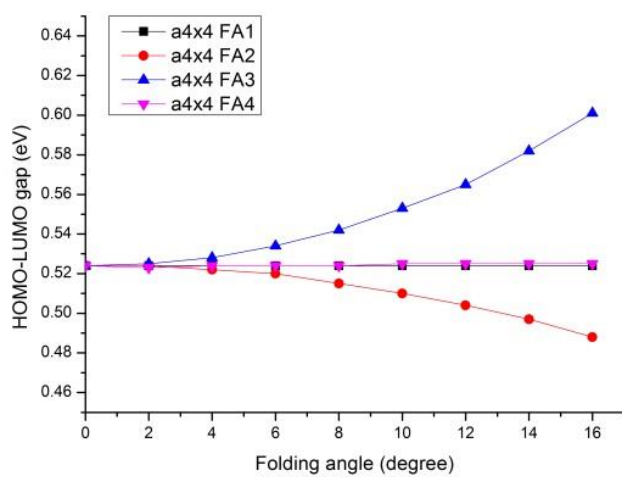
In Figure 4.1, the relation between HOMO-LUMO gaps of RGQDs with their sizes, folding axes, and folding angles were displayed. The variance of HOMO-LUMO gaps with folding angles is noticed and they differed from axis to axis. The more significant change on HOMO-LUMO gap was observed when structure is folded along FA3/FA2 axis for all sizes of RGQDs. However, the change is less when the structure is folded along FA1/FA4. Thus, the folding axis can be categorized into two main groups based on this behavior, i.e. FA2/FA3 and FA1/FA4 which is corresponded to the armchair- and the zigzag-like folding.



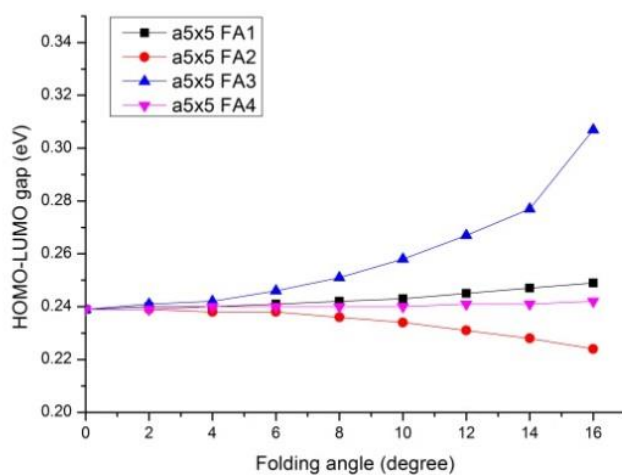
(a)



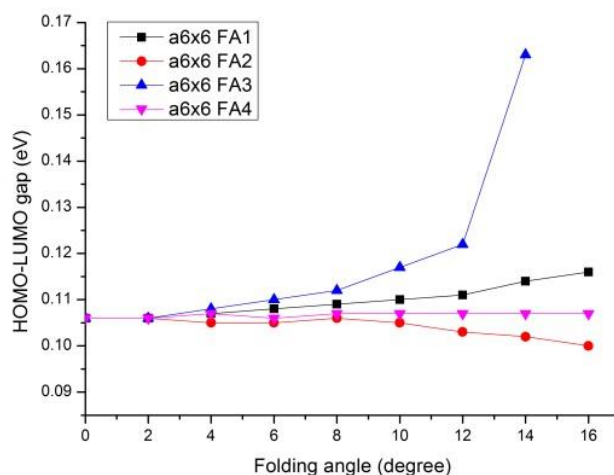
(b)



(c)



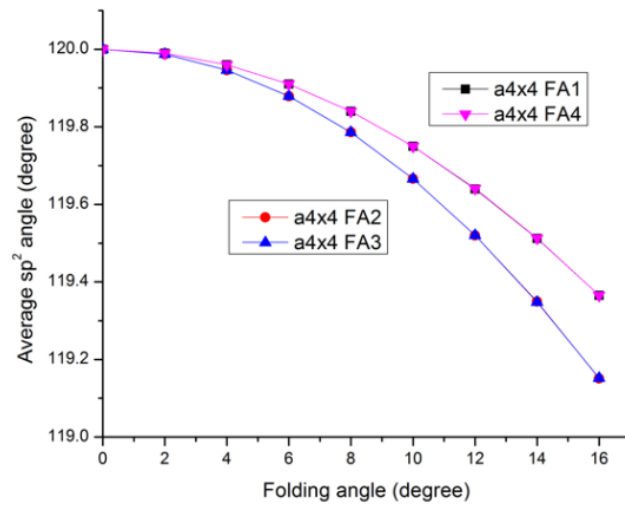
(d)



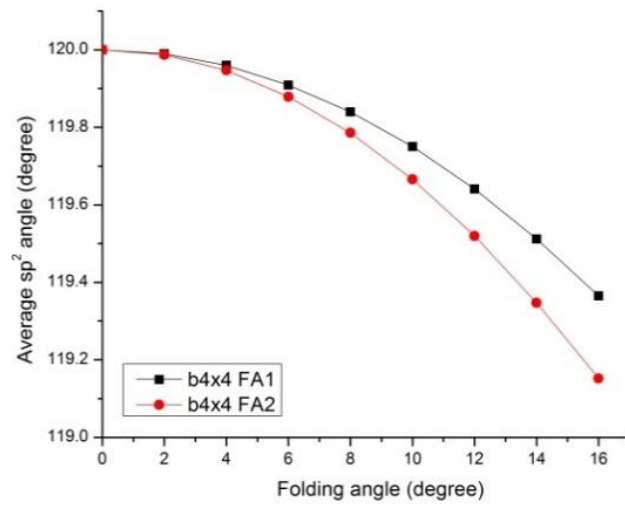
(e)

Figure 4.1 HOMO-LUMO gap as the function of folding angles; (a) a2x2 structures, (b) a3x3 structures, (c) a4x4 structures, (d) a5x5 structures, and (e) a6x6 structures

The similar relation to that appeared in Figure 4.1 was found between folding angles and average carbon-carbon angle (CCC) or sp^2 carbons (Csp^2) angles of the hexagonal ring, see Figure 4.2. Thus, FA2 and FA3 share the same average Csp^2 angle with the folding degree and like-wise for FA1 and FA4. Therefore, average Csp^2 angle can be used to distinguish between armchair- and zigzag-like folding. This average Csp^2 angle depends only on the folding axis but not with the size of RGQDs (see Table 4.1).



(a)



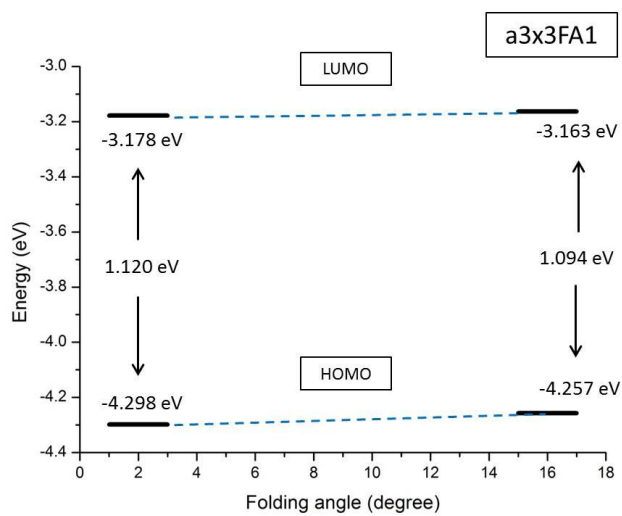
(b)

Figure 4.2 Relation between folding angle and average sp^2 angle; (a) rhomboidal-shape CGQDs of a4x4 and (b) hexagonal-shape CGQDs of b4x4

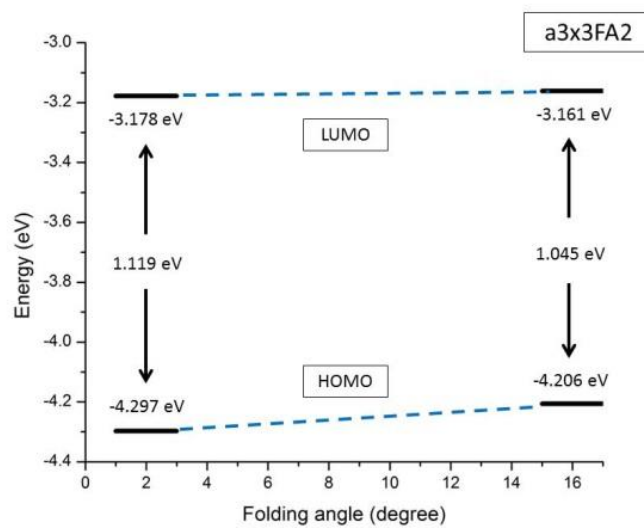
Table 4.1 Average sp^2 angle of rhomboidal-shape CGQDs

Folding axes	Folding angles (degree)	Average sp^2 angles (degree)				
		a2x2	a3x3	a4x4	a5x5	a6x6
FA1/FA4	0	120.000	120.000	120.000	120.000	120.000
	2	119.990	119.990	119.990	119.990	119.990
	4	119.960	119.960	119.960	119.960	119.960
	6	119.910	119.910	119.910	119.909	119.960
	8	119.839	119.839	119.840	119.839	119.840
	10	119.750	119.750	119.750	119.750	119.750
	12	119.641	119.640	119.640	119.641	119.640
	14	119.512	119.512	119.512	119.512	119.513
	16	119.365	119.365	119.365	119.365	119.366
FA2/FA3	0	120.000	120.000	120.000	120.000	120.000
	2	119.987	119.987	119.987	119.987	119.987
	4	119.946	119.946	119.946	119.946	119.946
	6	119.879	119.879	119.879	119.879	119.879
	8	119.786	119.786	119.786	119.785	119.786
	10	119.666	119.666	119.666	119.666	119.666
	12	119.520	119.520	119.520	119.520	119.520
	14	119.348	119.348	119.349	119.348	119.348
	16	119.152	119.151	119.151	119.152	119.151

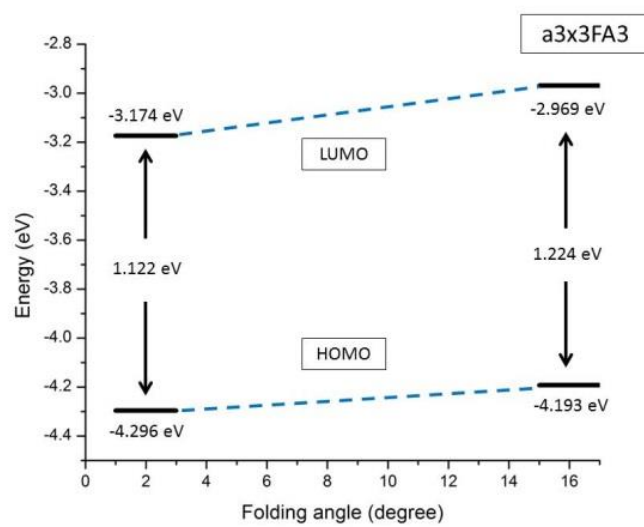
Our research has some different results from Zhang et. al. [28] who found that HOMO-LUMO gap becomes narrower for graphene nanoribbons with higher curvature. We observed the band gap reduction for most folding axes (FA1, FA2, and FA4), except for FA3 in which the band gap widening is noticed. To understand this phenomenon, we monitored HOMO/LUMO energies of a3x3 of the folding along four folding axes at 2 and 16 degree, Figure 4.3. Both HOMO and LUMO energies are destabilized upon the folding along for all folding axes. For FA3, the raise in LUMO is larger than HOMO and the HOMO-LUMO gap widening was observed. However, the increase in HOMO is larger than LUMO for FA1, FA2, and FA4 and the HOMO-LUMO gap narrowing is seen.



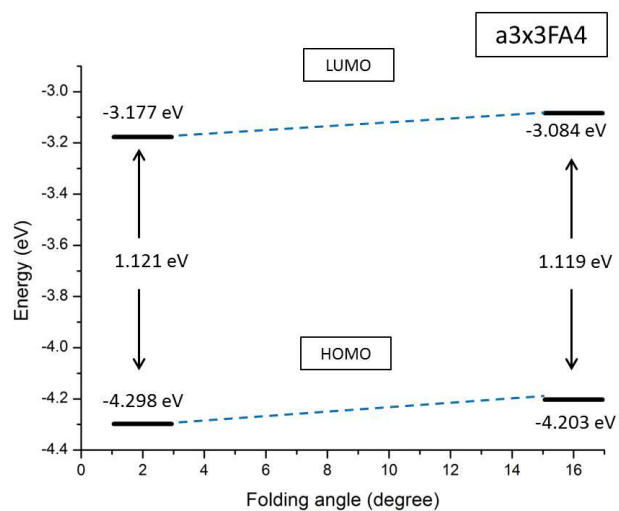
(a)



(b)

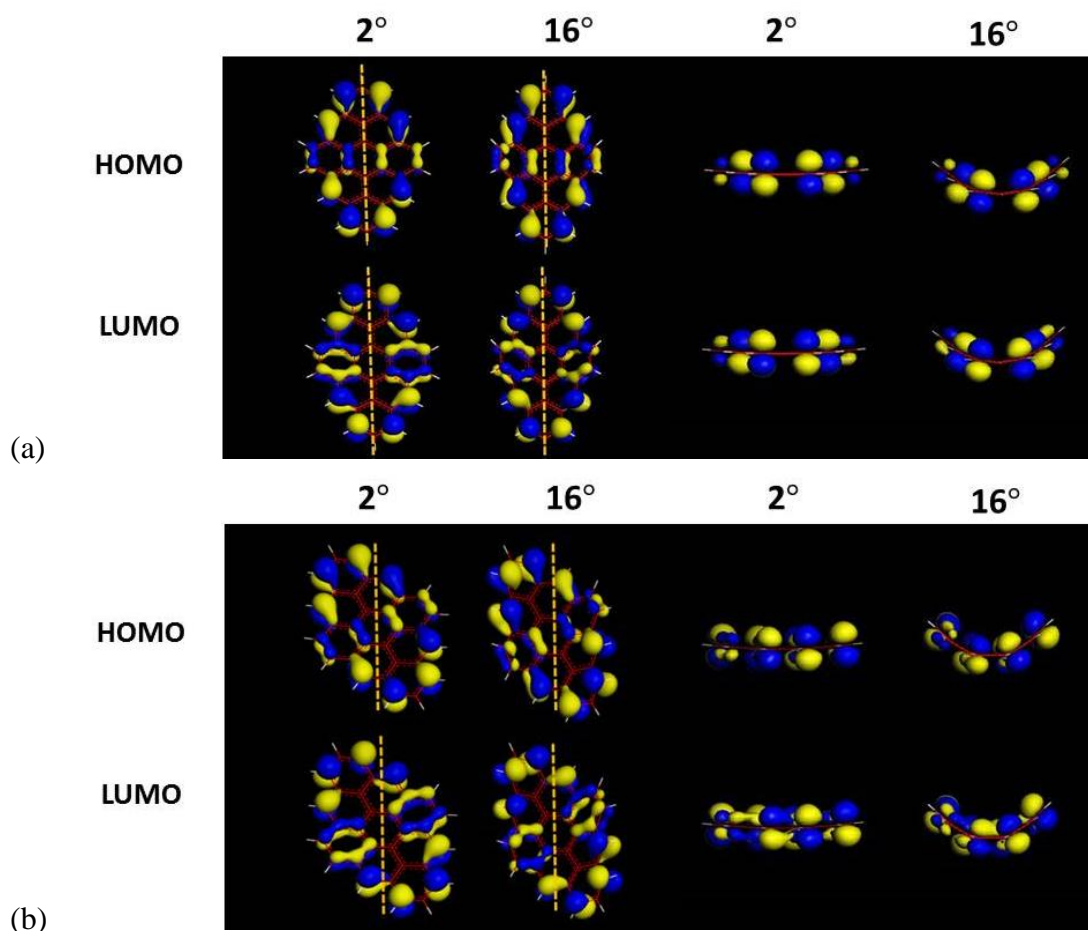


(c)



(d)

Figure 4.3 Comparison of HOMO and LUMO energies at 2 and 16 degrees of (a) a3x3FA1, (b) a3x3FA2, (c) a3x3FA3, and (d) a3x3FA4



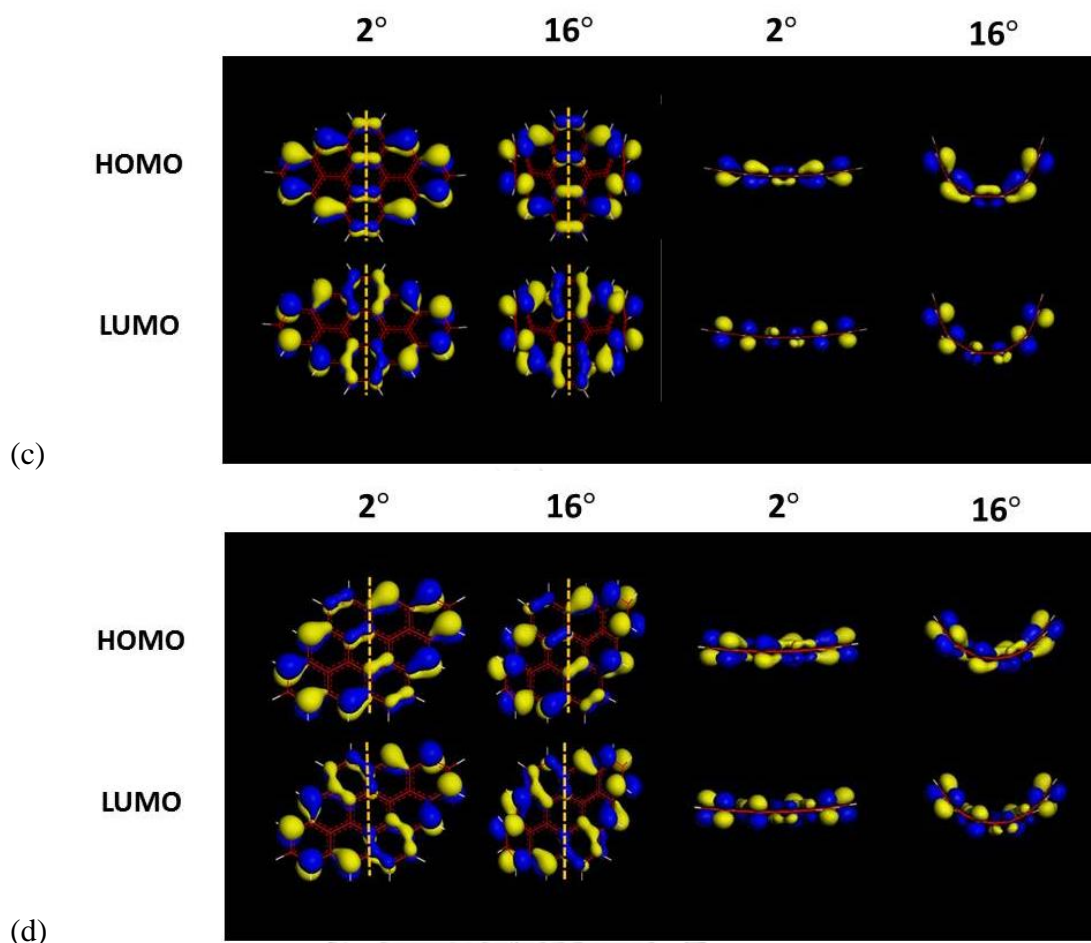


Figure 4.4 Illustrations of HOMO and LUMO orbitals of a3x3; (a) FA1, (b) FA2, (c) FA3, and (d) FA4

The destabilization of HOMO and LUMO with the folding degree can be understood through Figure 4.4. In the figure, yellow dotted line indicates the direction of folding axis that is at center of GQD, while yellow and blue colors of π orbitals denote the orbital phases. The π orbitals of HOMO/LUMO were brought towards each other when folded and this causes the destabilization of orbitals. For FA2, π orbitals in HOMO are positioned closer to each other, than those in LUMO. Therefore, HOMO is more destabilized than LUMO. For FA3, by the same argument as previous the stronger interaction of π orbitals is observed for LUMO than HOMO. Thus, the widening of HOMO-LUMO gap was observed.

From Figure 4.1 (e), we also observed the discontinuity of the HOMO-LUMO gap plot at the folding of 14° for FA3 of a6x6 RGQD. This discontinuity is the result of the strong orbital interaction between two ends of RGQD since the two ends are very close showed in Figure 4.5 (b). Whereas for FA2 at the same degree the two ends of RGQD still remain apart, Figure 4.5 (a), and the discontinuity was not seen. Additionally, for FA3 the folding at 16° could not be achieved since the two ends of RGQD will be overlaid and convergence solution could not be realized. The similar argument can also be used to describe Figure 4.1 (d).

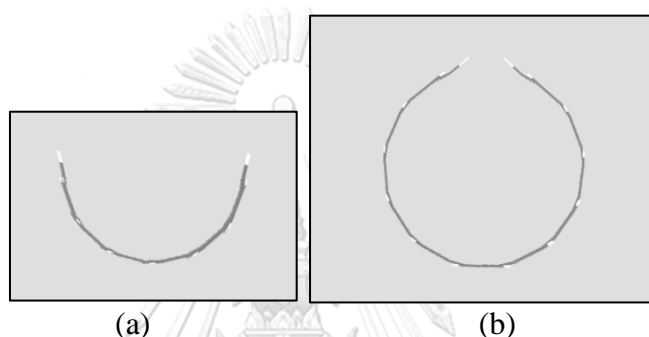


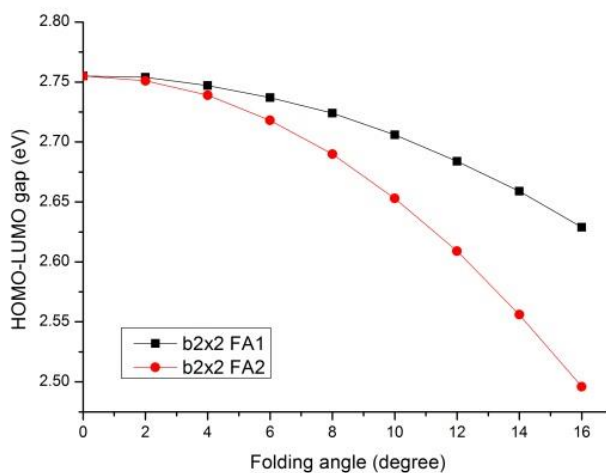
Figure 4.5 Side view structures of a6x6 at the folding angle of 14 degree when folded along (a) FA2 and (b) FA3.

4.1.1.2 Hexagonal CGQDs

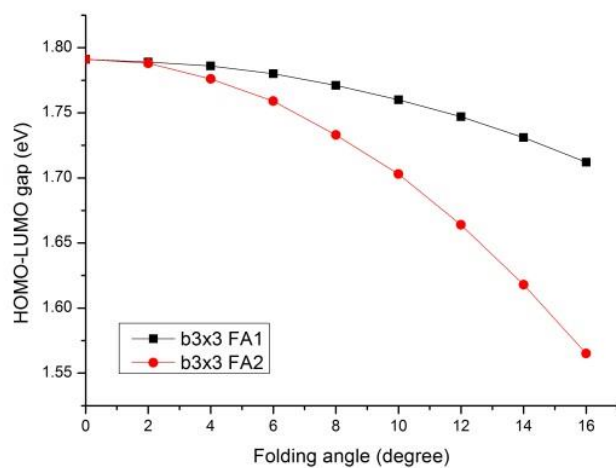
The average sp^2 angle of FA1 is larger than that of FA2 as demonstrated in Figure 4.2 (b). The zigzag- and armchair-like folding as given for FA1/FA4 and FA2/FA3 of RGQDs can be applied for the explanation. Like RGQDs, the average sp^2 angle for HGQDs did not depend on their sizes (see Table 4.2). When the folding angles were increased for both FA1 and FA2 at all quantum dot sizes, HOMO-LUMO gaps of HGQDs is reduced with folding angle for both FA1 and FA2. In spite of the HOMO-LUMO gap, the folding along FA2 decreases faster than FA1.

Table 4.2 Average sp^2 angle of hexagonal-shape CGQDs

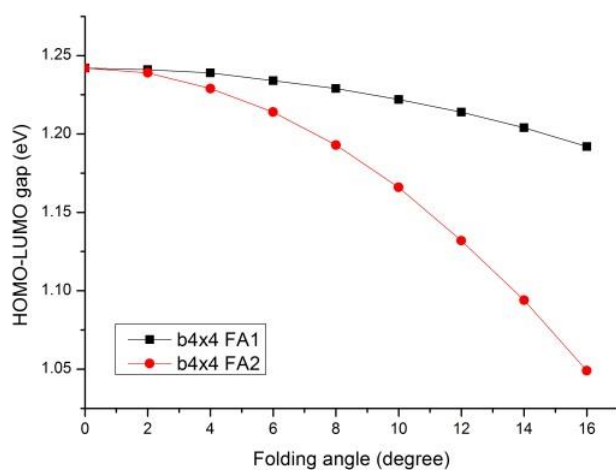
Folding axes	Folding angles (degree)	Average sp^2 angles (degree)				
		a2x2	a3x3	a4x4	a5x5	a6x6
FA1	0	120.000	120.000	120.000	120.000	120.000
	2	119.990	119.990	119.990	119.990	119.990
	4	119.960	119.960	119.960	119.960	119.960
	6	119.910	119.909	119.909	119.910	119.909
	8	119.839	119.839	119.840	119.839	119.839
	10	119.750	119.750	119.750	119.750	119.750
	12	119.640	119.641	119.641	119.641	119.641
	14	119.512	119.512	119.512	119.512	119.512
FA2	0	120.000	120.000	120.000	120.000	120.000
	2	119.987	119.987	119.987	119.987	119.987
	4	119.946	119.946	119.947	119.946	119.946
	6	119.879	119.879	119.879	119.879	119.879
	8	119.786	119.786	119.786	119.785	119.786
	10	119.666	119.665	119.666	119.666	119.666
	12	119.520	119.520	119.520	119.520	119.520
	14	119.348	119.347	119.347	119.348	119.348
	16	119.151	119.151	119.152	119.151	-



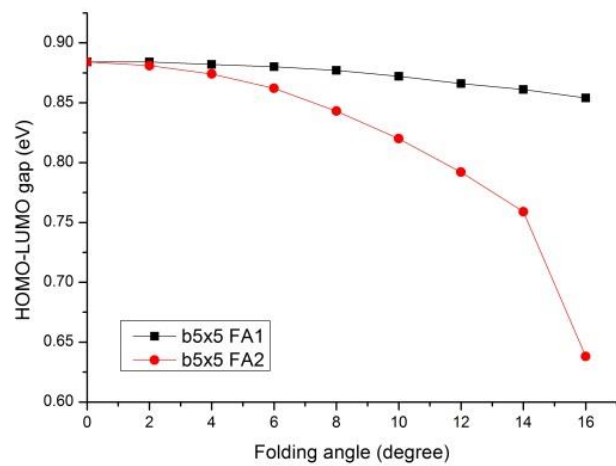
(a)



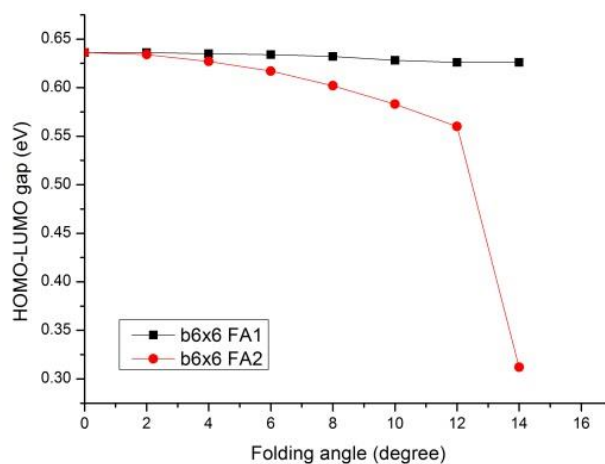
(b)



(c)



(d)



(e)

Figure 4.6 HOMO-LUMO gap change with folding angles; (a) b2x2 structures, (b) b3x3 structures, (c) b4x4 structures, (d) b5x5 structures, and (e) b6x6 structures

Like RGQDs, HOMO-LUMO gap of HGQDs is lowering because of the higher destabilization of HOMO as compared to LUMO for both FA1 and FA2, Figure 4.7. The greater increase of HOMO energy from the folding is related to the orbital interaction as demonstrated in Figure 4.8. The same discussion as given in the previous section can be as well used.

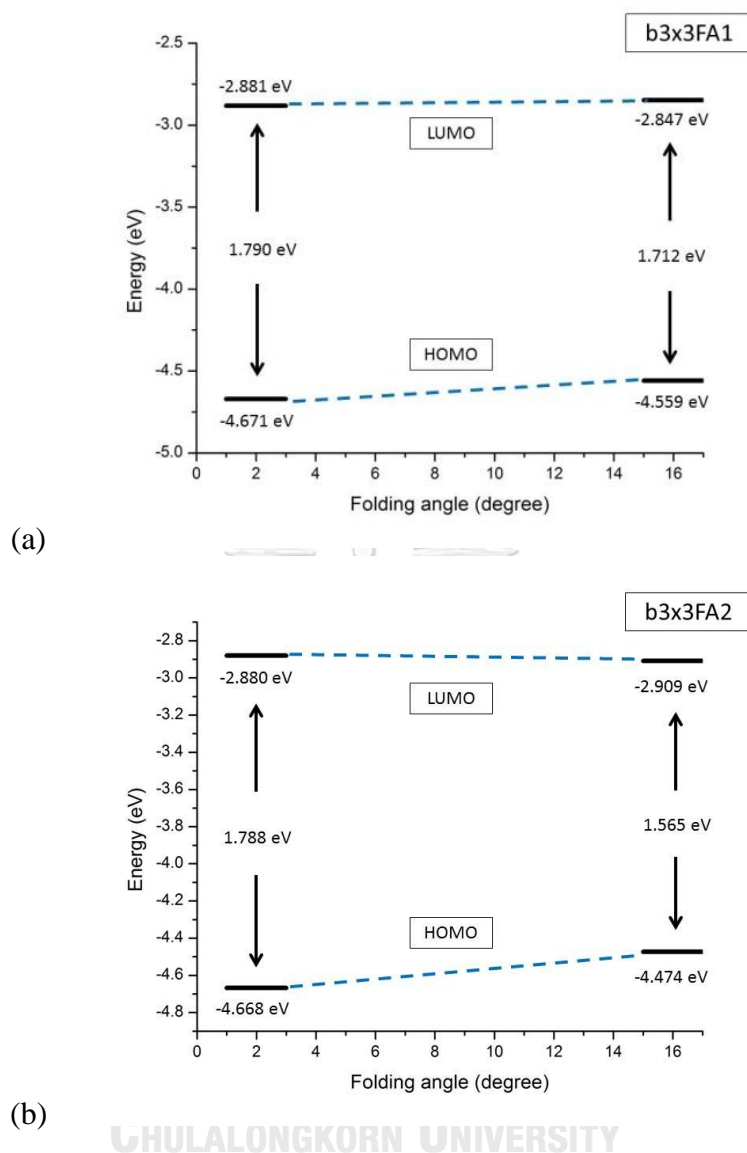


Figure 4.7 Comparison of HOMO and LUMO energies at 12 and 14 degrees of
(a) b3x3FA1 and (b) b3x3FA2

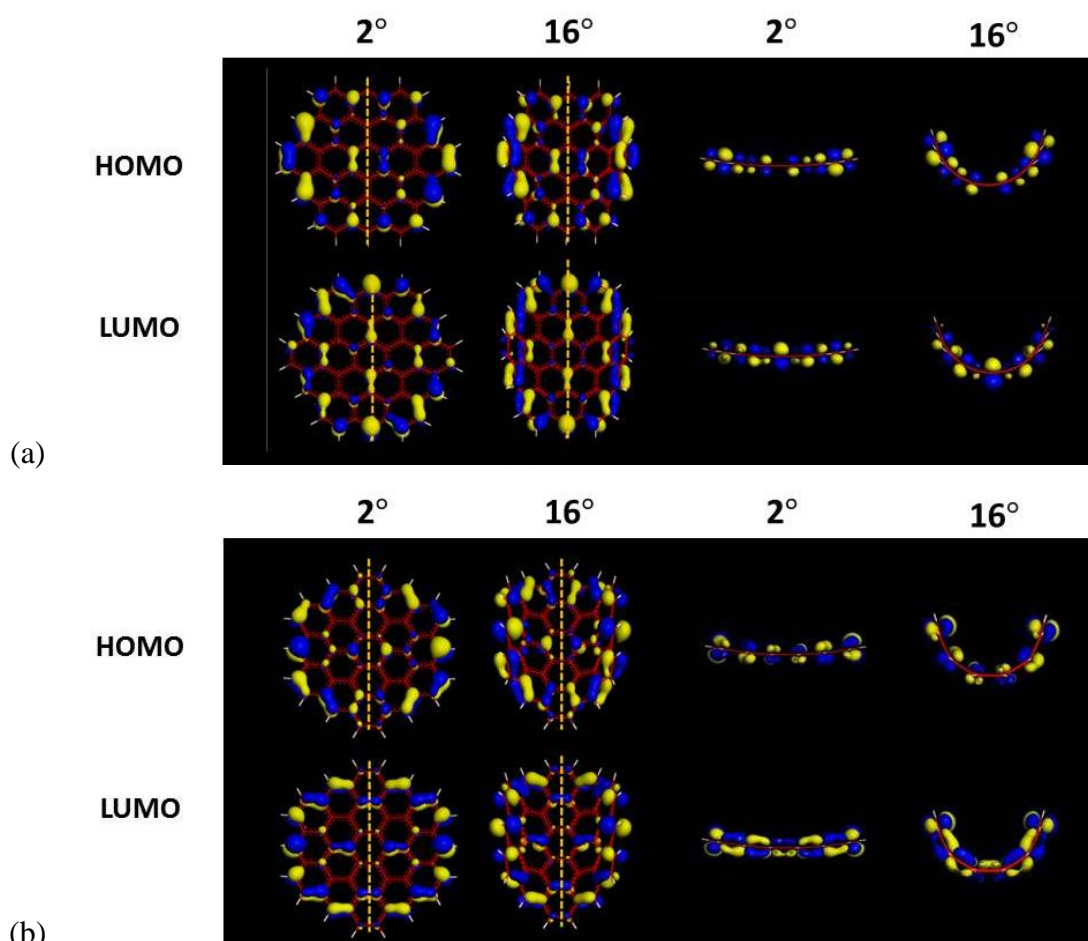
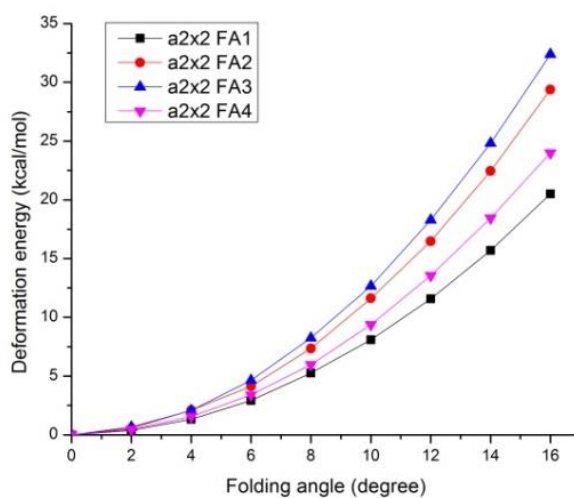


Figure 4.8 Comparison of HOMO and LUMO of b3x3; (a) FA1 and (b) FA2

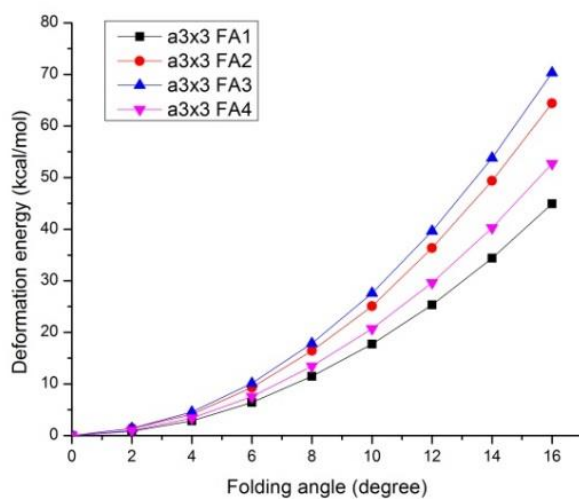
Similar to RGQDs, the large HGQDs (b5x5 and b6x6) had the discontinuity in HOMO-LUMO gaps. We expect the same reasoning as RGDQs for this behavior.

4.1.2 Deformation Energies

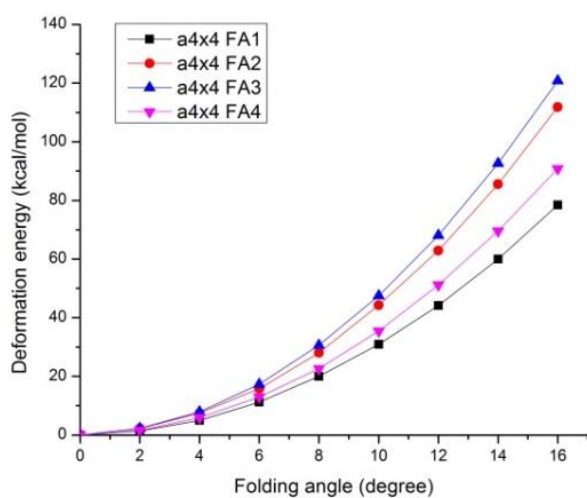
The different between the total energy of CGQD and flat GQD is defined as the deformation energy. The value shows the ease of curving GQDs along a specific folding axis. The relations between deformation energies and folding angles for several folding axes of RGQDs and HGQDs were exhibited in Figure 4.9 and 4.10, respectively.



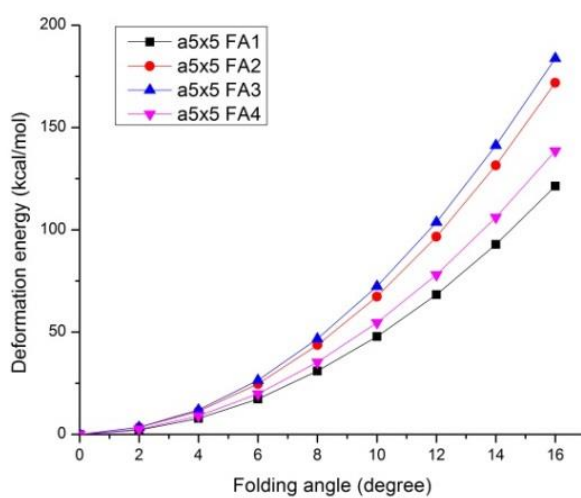
(a)



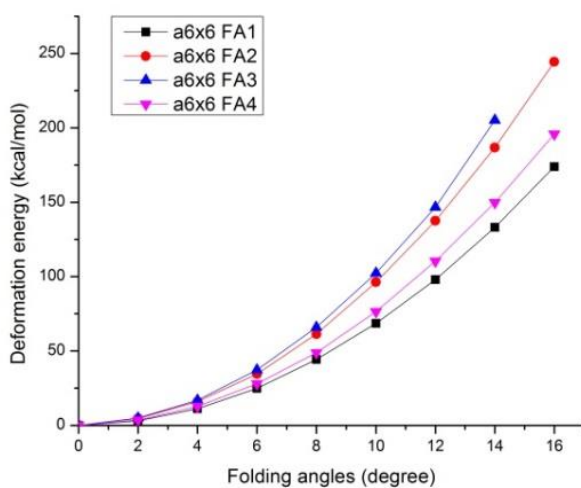
(b)



(c)



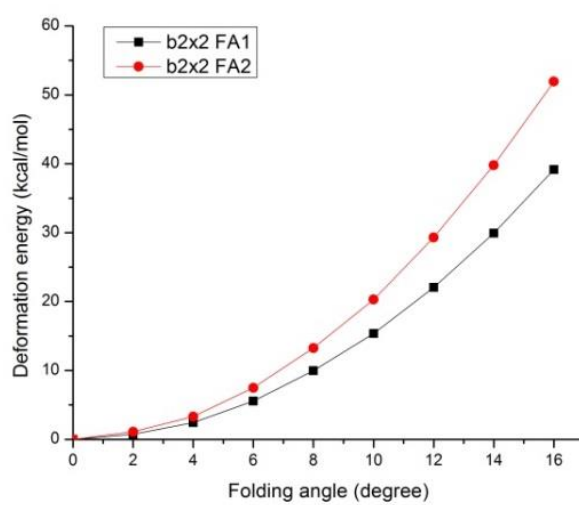
(d)



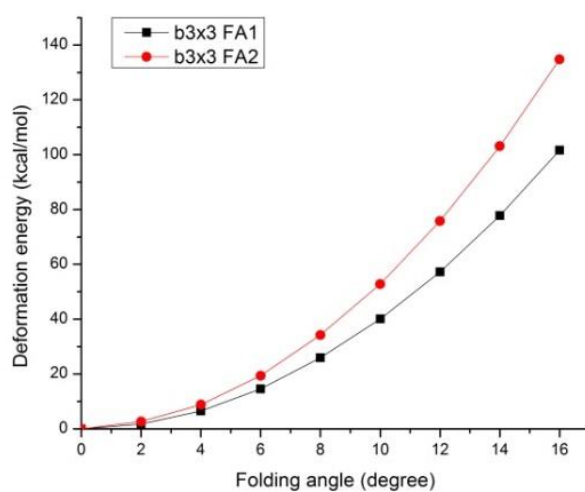
(e)

CHULALONGKORN UNIVERSITY

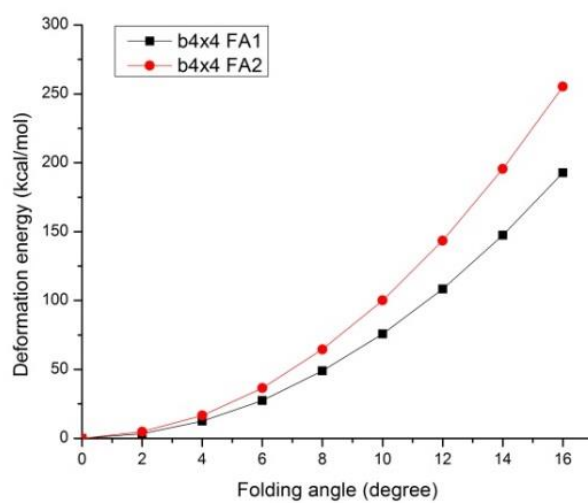
Figure 4.9 Deformation energies for different folding axes of RGQDs at various folding angles; (a) a2x2 structures, (b) a3x3 structures, (c) a4x4 structures, (d) a5x5 structures, and (e) a6x6 structures



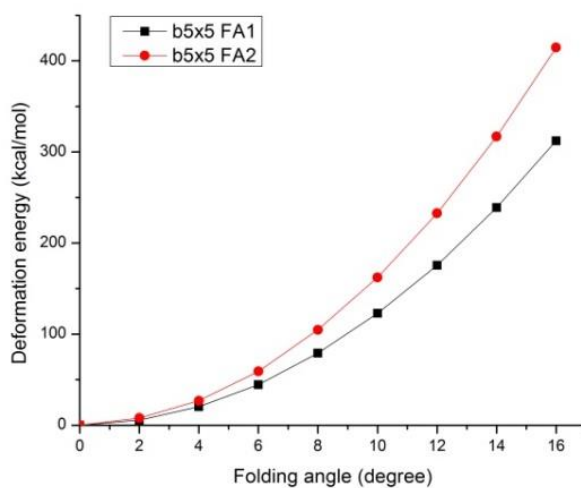
(a)



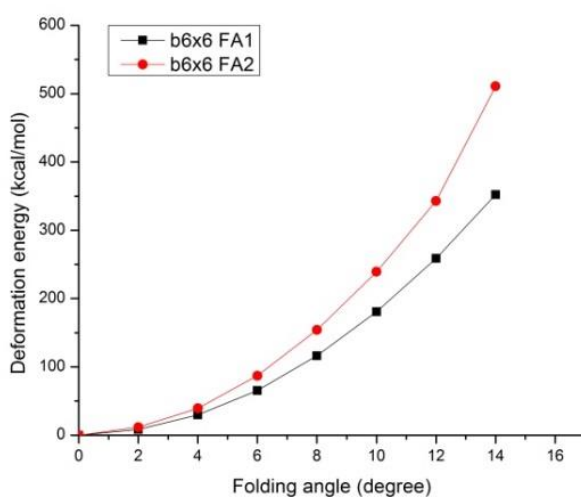
(b)



(c)



(d)



(e)

Figure 4.10 Deformation energies for different folding axes of HGQDs at various folding angles; (a) b2x2 structures, (b) b3x3 structures, (c) b4x4 structures, (d) b5x5 structures, and (e) b6x6 structures

Chang et.al. [29] reported that the deformation energy of graphene nanoribbons would increase when the folding angle is enhanced. Similarly, our results revealed that the deformation energy is raised with the degree of folding along all folding axes for all GQDs sizes. Interestingly, the plot between deformation energies and folding angles is harmonic ($R^2 \sim 0.99$ when fits with the quadratic equation). The

deformation energy also depends the folding axis. The bending along armchair-like folding axis (FA2, FA3 for RGQDs and FA2 for HGQDs) requires more energy than that along the zigzag-like folding axis (FA1, FA4 for RGQDs and FA1 for HGQDs). It is possible that the armchair-like folding generates higher “folding” strain. Since the angle of carbon-carbon bond (CCC angle) make 30° for the armchair-like folding, while for the zigzag-like folding it makes 60° , see Figure 3.2. The deformation energies at 16° for FA2 of RGQDs, FA3 of RGQDs, and FA2 of HGQDs were plotted with number of C atoms together on the same graph, and the linear relation with R^2 of 0.9977 was obtained, Figure 4.11. Likewise, the deformation energies at 16° for FA1 of RGQDs, FA4 of RGQDs, and FA1 of HGQDs were plotted together with number of C atoms. Similar linear relation with $R^2 = 0.9922$ was found, Figure 4.11. This shows that the deformation energy for the same type of folding axis varies only with the size of GQDs, but not on their shape. The increase of deformation energy with the size of GQDs can be explained by numbers of the symmetry-unique axis. The bigger size GQD has higher numbers of the symmetry-unique axis and thus larger deformation energies.

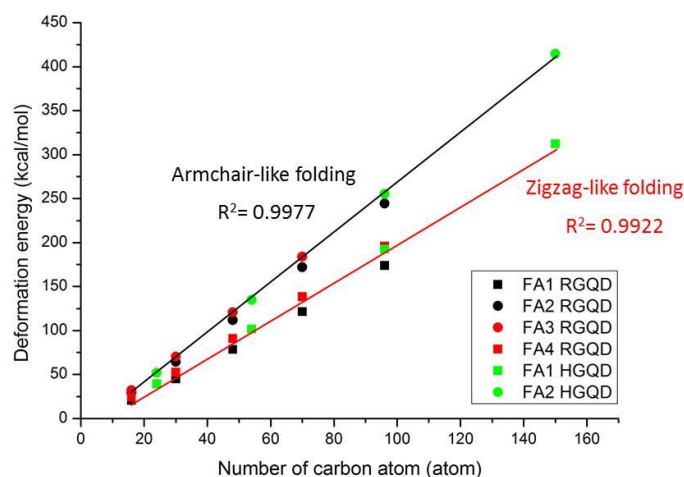


Figure 4.11 Relation between deformation energies at 16° and numbers of carbon atoms for FA2 of RGQDs, FA3 of RGQDs, FA2 of HGQDs, FA1 of RGQDs, FA4 of RGQDs, and FA1 of HGQDs.

4.2 Adsorptions of lithium atom/ion on graphene quantum dots

4.2.1 One-Li-ion system

The adsorption of one Li ion on b2x2, b3x3, and b4x4 GQDs with negative charge ($q=-1$), neutral charge ($q=0$), and positive charge ($q=1$) was studied. For b2x2 GQD ($C_{24}H_{12}$), there are two distinct adsorbed sites, while b3x3 ($C_{54}H_{18}$) and b4x4 ($C_{96}H_{24}$) GQDs have four and six distinct sites, respectively, see Figure 4.12. Adsorption energies of Li^+ on GQDs were displayed in Table 4.3.

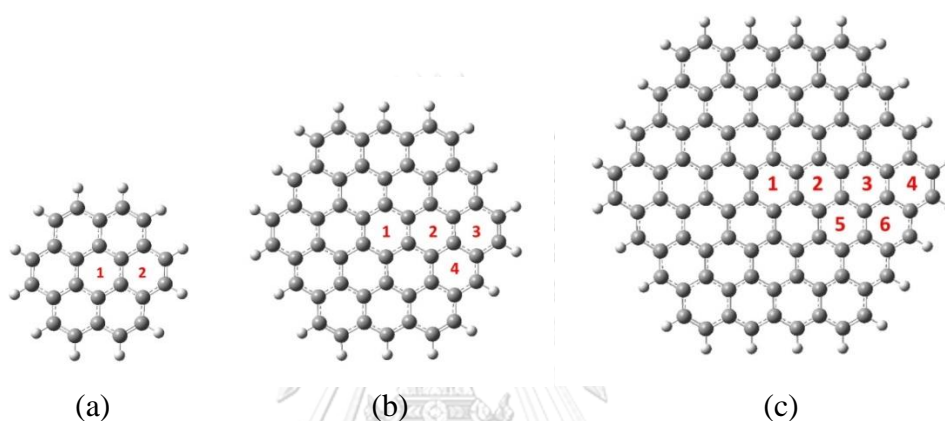


Figure 4.12 Lithium positions on three GQDs; (a) $C_{24}H_{12}$, (b) $C_{54}H_{18}$, and (c) $C_{96}H_{24}$.

Table 4.3 Adsorption energies in kcal/mol of one Li ion on GQDs with negative ($q = -1$), neutral ($q = 0$), and positive ($q=1$) charge at various adsorbed sites.

GQDs	Positions	Adsorption energies (kcal/mol)		
		GQD ($q=-1$)	GQD ($q=0$)	GQD ($q=1$)
$C_{24}H_{12}$	1	-130.235	-47.780	32.560
	2	-135.073	-49.466	28.552
$C_{54}H_{18}$	1	-115.225	-51.803	8.823
	2	-115.251	-50.923	7.012
	3	-118.309	-51.905	3.598
	4	-118.996	-52.765	3.871
$C_{96}H_{24}$	1	-103.809	-54.061	-6.363
	2	-105.837	-54.714	-8.292
	3	-106.192	-55.016	-9.055
	4	-108.924	-54.803	-10.982
	5	-106.455	-54.941	-7.748
	6	-111.703	-56.929	-12.125

For all sizes and charges of GQDs, the adsorption of Li^+ at the outermost circle of GQDs is the most preferable and at the center of GQDs is the least. Notice that for $\text{C}_{96}\text{H}_{24}$ the position 4 and 6 are at the outermost circle. This behavior could be explained by electrostatic interaction between Li ion and GQDs. Table 4.4 shows Mulliken net charge of Li ion, six-membered (C_6) ring of GQD, and total GQD. It can be seen that the C_6 charge at the outermost circle position is more negative than at the central position which lead to strong interaction. This relation is in agreement with the adsorption energies shown in Table 4.3.

Table 4.4 Net charges of lithium ion, C_6 ring of GQD, and total GQD.

GQDs	Positions	Charges (atomic unit)								
		GQD (q=-1)			GQD (q=0)			GQD (q=1)		
		Li^+	C_6	GQD	Li^+	C_6	GQD	Li^+	C_6	GQD
$\text{C}_{24}\text{H}_{12}$	1	0.424	-0.248	-0.424	0.537	-0.179	0.463	0.629	-0.172	1.371
	2	0.349	-0.418	-0.349	0.471	-0.361	0.529	0.574	-0.360	1.426
$\text{C}_{54}\text{H}_{18}$	1	0.464	-0.134	-0.464	0.519	-0.102	0.481	0.584	-0.104	1.416
	2	0.459	-0.213	-0.459	0.524	-0.195	0.476	0.572	-0.183	1.428
	3	0.376	-0.396	-0.376	0.468	-0.379	0.532	0.530	-0.364	1.470
	4	0.401	-0.297	-0.401	0.473	-0.266	0.527	0.531	-0.260	1.469
$\text{C}_{96}\text{H}_{24}$	1	0.491	-0.249	-0.492	0.532	-0.250	0.468	0.559	-0.232	1.441
	2	0.485	-0.223	-0.485	0.522	-0.203	0.478	0.552	-0.194	1.448
	3	0.466	-0.250	-0.466	0.510	-0.237	0.49	0.541	-0.229	1.459
	4	0.388	-0.385	-0.388	0.469	-0.387	0.531	0.507	-0.374	1.493
	5	0.476	-0.232	-0.476	0.524	-0.221	0.476	0.554	-0.208	1.446
	6	0.416	-0.282	-0.416	0.469	-0.268	0.531	0.502	-0.263	1.498

As expected, the binding of Li^+ to negative charge GQDs is the strongest with the binding affinity greater than 100 kcal/mol. Of course, this is due to strong electrostatic attraction between Li^+ and negative charged GQDs. The binding becomes weaker as the charge of GQDs being more positive. For negative charge GQDs, the smaller size GQDs have the stronger interaction, $\text{C}_{24}\text{H}_{12} > \text{C}_{54}\text{H}_{18} > \text{C}_{96}\text{H}_{24}$. However, the reverse is found for neutral and positive charge GQDs. This observation is somehow in line with the product of Li^+ and total GQD charge in Table 4.4. The product of Li^+ and positive $\text{C}_{24}\text{H}_{12}$ charges is the largest and hence large positive interaction energy was found. Notice that Li^+ charge is not +1, but approximately 0.5 for all cases. This suggests that GQD, no matter what charge condition, donates electrons to Li ion. However, the electron donating capability of GQDs depends on the charge of GQD more than its size. The the electron donating

capability of GQDs is reduced, when the GQD becomes more positive as evident by the increase of Li^+ charge.

4.2.2 Two-Li-ion system

To investigate the packing of Li ion on GQDs, we looked at the adsorption of multiple Li ions on $\text{C}_{24}\text{H}_{12}$ and $\text{C}_{54}\text{H}_{18}$ with various charges. The adsorption patterns for the two Li-ion system on GQDs were given in Table 3.3 and corresponding binding affinities were listed in Table 4.5. There are 4 and 15 patterns for $\text{C}_{24}\text{H}_{12}$ and $\text{C}_{54}\text{H}_{18}$, respectively.

Table 4.5 Adsorption energies per ion of two Li-ion on $\text{C}_{24}\text{H}_{12}$ and $\text{C}_{54}\text{H}_{18}$ with various charges.

GQDs	Patterns	Adsorption energies (kcal/mol)		
		-1	0	1
$\text{C}_{24}\text{H}_{12}$	1	-94.548	-15.285	56.324
	2	-94.458	-15.285	NC
	3	-96.473	-13.659	57.542
	4	-96.509	-15.285	56.324
$\text{C}_{54}\text{H}_{18}$	1	NC	-27.831	28.519
	2	NC	-26.559	30.512
	3	-83.817	-21.340	27.073
	4	-85.403	-22.573	35.618
	5	-85.264	-26.678	29.330
	6	-88.307	-23.707	30.218
	7	-89.247	-26.677	28.599
	8	-89.474	-28.239	27.073
	9	-90.134	-29.131	27.375
	10	-90.100	-29.273	26.709
	11	NC	-23.259	34.085
	12	-85.952	-21.862	33.886
	13	-87.626	-25.479	30.675
	14	-88.283	-26.558	30.512
	15	-86.537	-23.256	34.133

*NC = No converged result

From Table 4.5, the adsorption energy of two-Li-ion system is less than the one-ion system for all sizes. The reason for the weaker interaction is likely due to be the repulsion between Li ions. Figure 4.13 illustrates the linear relation between binding affinity and reciprocal Li-Li distance ($1/R$). If distance between two Li ions is short, it will result in weak adsorption. This suggests the important of Li-Li repulsion for this system. The result in Table 4.6 also implies that the packing of two Li-ion is favorable for GQDs with negative charge but not for neutral and positive charge GQDs. Thus, during charging the GQD attracts Li^+ while during discharging it repels Li^+ .

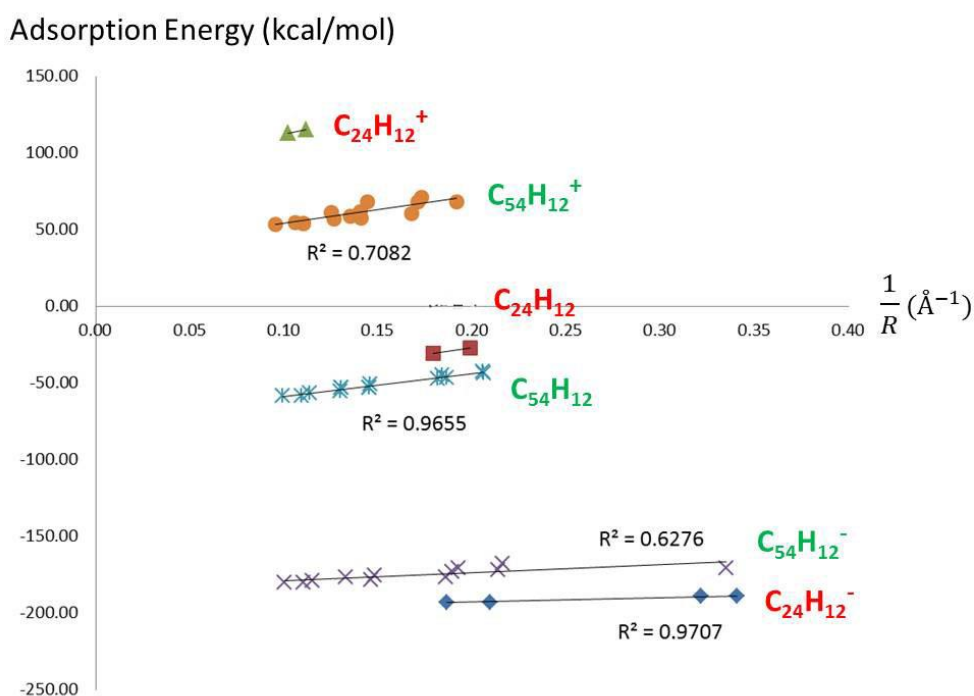


Figure 4.13 Relation between $1/R$ and adsorption energies of GQD- 2Li^+ complexes

4.2.3 One-Li-atom system

In the charging situation, Li^+ will receive electron and become Li atom. The adsorption of Li atom on GQDs with various charges is also of interest. Using the same adsorbed sites as one-Li-ion system adsorption energies of Li atom on $\text{C}_{24}\text{H}_{12}$, $\text{C}_{54}\text{H}_{18}$, and $\text{C}_{96}\text{H}_{24}$ with various charges were given in Table 4.6.

Table 4.6 Adsorption energies of Li atom on $C_{24}H_{12}$, $C_{54}H_{18}$, and $C_{96}H_{24}$ with $q = -1$, $q=0$, and $q = 1$.

GQDs	Positions	Adsorption energies (kcal/mol)		
		GQD ($q=-1$)	GQD ($q=0$)	GQD ($q=1$)
$C_{24}H_{12}$	1	-3.622	-8.315	-21.965
	2	-8.697	-13.152	-25.254
$C_{54}H_{18}$	1	-15.311	-16.228	-23.990
	2	-14.761	-16.360	-24.419
	3	-17.200	-19.312	-28.554
	4	-18.111	-19.999	-28.625
$C_{96}H_{24}$	1	-21.966	-20.959	-27.180
	2	-20.925	-22.987	-28.587
	3	-22.231	-23.395	-28.726
	4	-23.989	-26.074	-31.964
	5	-21.980	-23.608	-23.286
	6	-25.982	-28.853	-31.842

The result in Table 4.7 is opposite to the one-Li-ion system. The binding of Li atom with the positive GQD is the strongest and with the negative GQD is the weakest. Thus, during discharging condition GQD attract Li atom more strongly than during charging. However, the adsorption energy for one-Li-atom system is smaller than that for one-Li-ion. The binding also increases with the size of GQDs. ($C_{96}H_{24} > C_{54}H_{18} > C_{24}H_{12}$) Still, there is a preference of adsorption at outermost circle. The behavior can also be explained by the C_6 charge of GQDs. Charges of Li atom and C_6 charge of GQDs are listed in Table 4.7. The results suggest that C_6 charges of outermost circle are more negative than the center and other position, especially C_6 charge at the corner of the outermost circle. It directly relates with adsorption energy.

Table 4.7 Net charges of lithium atom and C₆ of Li-GQD complexes

GQDs	Positions	Charges (atomic unit)					
		GQD (q=-1)		GQD (q=0)		GQD (q=1)	
		Li	C ₆	Li	C ₆	Li	C ₆
C ₂₄ H ₁₂	1	0.324	-0.307	0.424	-0.248	0.509	-0.243
	2	0.242	-0.429	0.349	-0.418	0.455	-0.406
C ₅₄ H ₁₈	1	0.418	-0.162	0.464	-0.134	0.526	-0.114
	2	0.406	-0.241	0.459	-0.213	0.514	-0.197
	3	0.320	-0.380	0.376	-0.396	0.435	-0.394
	4	0.347	-0.308	0.401	-0.297	0.468	-0.287
C ₉₆ H ₂₄	1	0.457	-0.249	0.492	-0.249	0.518	-0.230
	2	0.456	-0.237	0.485	-0.223	0.516	-0.205
	3	0.435	-0.267	0.466	-0.250	0.508	-0.238
	4	0.351	-0.376	0.388	-0.385	0.429	-0.390
	5	0.443	-0.241	0.476	-0.232	0.504	-0.220
	6	0.381	-0.284	0.416	-0.282	0.456	-0.273



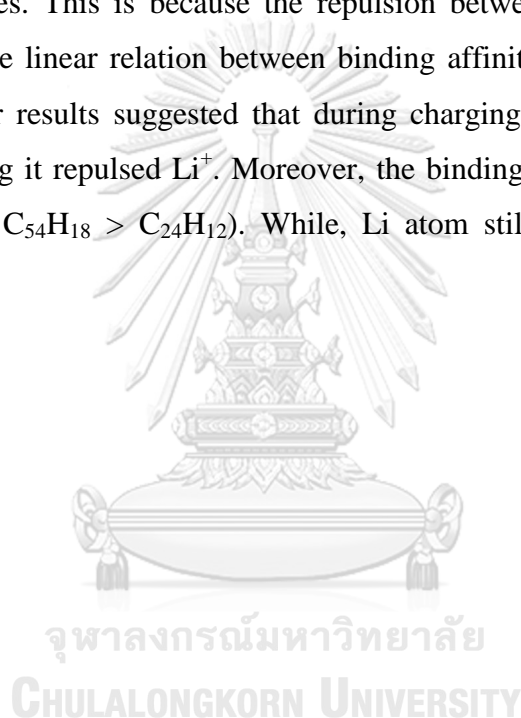
CHAPTER V

CONCLUSIONS

Theoretical study on the electronic properties of two shapes of curved graphene quantum dots, rhomboidal-CGQDs and hexagonal-CGQDs, by PBE/DNP revealed that shapes, sizes, folding axes, and degrees of folding affected the HOMO/LUMO energies and band gaps of CGQDs. The observed band gap of CGQDs decreases when the folding angle is increased for all folding axes except for by FA3 of RGQDs. The changes of band gap and HOMO/LUMO energies can be explained by the orbital interactions. It was found that HOMO/LUMO are destabilized upon folding for FA3 of RGQDs, the folding destabilizes LUMO more than HOMO and hence the widening of the band gaps was found. In other case, HOMO was destabilized than LUMO. The π orbitals with different phases are put closer to each other when folded. This causes the destabilization of orbital. Thus, the narrowing of band gap was found. The orbital interactions are varied with the folding axis and the band gap behavior upon folding is different. The armchair-like folding (FA2/FA3 of RGQDs and FA2 of HGQDs) causes the band gap to change more significantly than the zigzag-like folding, FA4 and FA1 of RGQDs and FA1 of HGQDs. Moreover, the deformation energy of CGQDs is depended on the size and folding axis but not the shape of GQDs.

The adsorption lithium atom/ion adsorption on flat GQDs (coronene $C_{24}H_{12}$, circumcoronene $C_{54}H_{18}$, and circumcircumcoronene $C_{96}H_{24}$) at various charge conditions and adsorption positions were investigated using M06-2X/6-31g(d). The adsorption of one Li/Li⁺ on GQDs had two, four, and six distinct adsorbed sites for $C_{24}H_{12}$, $C_{54}H_{18}$, and $C_{96}H_{24}$, respectively. For the adsorptions of Li⁺/Li on GQDs, Li⁺/Li is favored to bind at the outermost circle of GQDs more than at the center. The result can be explained by the electrostatic interaction between a Li⁺/Li and GQDs. We found that the charge of six-membered ring at the outermost circle is more negative than at the central. This distribution of charges is related to the adsorption energy. Li⁺ most strongly binds to negative GQDs with the energy of greater than 100 kcal/mol. The smaller size of negative GQDs has the stronger interaction than the

larger one, $C_{24}H_{12} > C_{54}H_{18} > C_{96}H_{24}$. However, the opposite results were found for neutral and positive GQDs. The product of Li^+ and GQD charge is the most positive for positive $C_{24}H_{12}$, thus Li^+ has an the most unfavorable interaction with it. The Li^+ charge is approximately 0.5, which suggested GQD donating electrons to Li ion. The degree of donation depends on the charge of GQD more than its size. In one-lithium-atom system, the result is opposite to the one-Li-ion system. The adsorption of Li atom on positive GQDs is the strongest, while on negative GQDs ($q=-1$) is the weakest. Adsorption energies per Li^+ of two-Li-ion system are less than the one-ion system for all sizes. This is because the repulsion between Li ions, which can be illustrated from the linear relation between binding affinity and the reciprocal Li-Li distance ($1/R$). Our results suggested that during charging GQDs attracts Li^+ , while during discharging it repulsed Li^+ . Moreover, the binding increases with the size of GQDs ($C_{96}H_{24} > C_{54}H_{18} > C_{24}H_{12}$). While, Li atom still prefers to adsorb at the outermost circle.



REFERENCES

- [1] Castro Neto, A. H., Guinea, F., Peres, N. M. R., Novoselov, K. S., and Geim, A. K. The electronic properties of graphene. Reviews of Modern Physics 81 (1) (2009): 109-162.
- [2] Allen, M. J., Tung, V. C., and Kaner, R. B. Honeycomb carbon: A review of graphene. Chemical Reviews 110 (1) (2010): 132-145.
- [3] Xu, M., Liang, T., Shi, M., and Chen, H. Graphene-like two-dimensional materials. Chemical Reviews 113 (5) (2013): 3766-3798.
- [4] Banhart, F., Kotakoski, J., and Krasheninnikov, A. V. Structural defects in graphene. ACS Nano 5 (1) (2011): 26-41.
- [5] Novoselov, K. S., Geim, A. K., Morozov, S. V., Jiang, D., Katsnelson, M. I., Grigorieva, I. V., Dubonos, S. V., and Firsov, A. A. Two-dimensional gas of massless Dirac fermions in graphene. Nature 438 (2005): 197.
- [6] Geim, A. K., and Novoselov, K. S. The rise of graphene. Nature Materials 6 (2007): 183.
- [7] Geim, A. K. Graphene: Status and prospects. Science 324 (5934) (2009): 1530.
- [8] Zhang, Z., Zhang, J., Chen, N., and Qu, L. Graphene quantum dots: an emerging material for energy-related applications and beyond. Energy & Environmental Science 5 (10) (2012): 8869-8890.
- [9] Bacon, M., Bradley Siobhan, J., and Nann, T. Graphene quantum dots. Particle & Particle Systems Characterization 31 (4) (2013): 415-428.
- [10] Liu, W. W., Feng, Y. Q., Yan, X. B., Chen, J. T., and Xue, Q. J. Superior micro-supercapacitors based on graphene quantum dots. Advanced Functional Materials 23 (33) (2013): 4111-4122.
- [11] Chao, D., Zhu, C., Xia, X., Liu, J., Zhang, X., Wang, J., Liang, P., Lin, J., Zhang, H., Shen, Z. X., and Fan, H. J. Graphene quantum dots coated VO₂ arrays for highly durable electrodes for Li and Na ion batteries. Nano Letters 15 (1) (2015): 565-573.
- [12] Pan, D., Xi, C., Li, Z., Wang, L., Chen, Z., Lu, B., and Wu, M. Electrophoretic fabrication of highly robust, efficient, and benign heterojunction

- photoelectrocatalysts based on graphene-quantum-dot sensitized TiO₂ nanotube arrays. Journal of Materials Chemistry A 1 (11) (2013): 3551-3555.
- [13] Shen, J., Zhu, Y., Yang, X., and Li, C. Graphene quantum dots: emergent nanolights for bioimaging, sensors, catalysis and photovoltaic devices. Chemical Communications 48 (31) (2012): 3686-3699.
- [14] Zhu, S., Zhang, J., Qiao, C., Tang, S., Li, Y., Yuan, W., Li, B., Tian, L., Liu, F., Hu, R., Gao, H., Wei, H., Zhang, H., Sun, H., and Yang, B. Strongly green-photoluminescent graphene quantum dots for bioimaging applications. Chemical Communications 47 (24) (2011): 6858-6860.
- [15] Li, M., Ni, W., Kan, B., Wan, X., Zhang, L., Zhang, Q., Long, G., Zuo, Y., and Chen, Y. Graphene quantum dots as the hole transport layer material for high-performance organic solar cells. Physical Chemistry Chemical Physics 15 (43) (2013): 18973-18978.
- [16] Ritter, K. A., and Lyding, J. W. The influence of edge structure on the electronic properties of graphene quantum dots and nanoribbons. Nature Materials 8 (2009): 235.
- [17] Nakada, K., Fujita, M., Dresselhaus, G., and Dresselhaus, M. S. Edge state in graphene ribbons: Nanometer size effect and edge shape dependence. Physical Review B 54 (24) (1996): 17954-17961.
- [18] Eda, G., Lin, Y. Y., Mattevi, C., Yamaguchi, H., Chen, H. A., Chen, I. S., Chen, C. W., and Chhowalla, M. Blue photoluminescence from chemically derived graphene oxide. Advanced Materials 22 (4) (2009): 505-509.
- [19] Kuamit, T., Ratanasak, M., Rungnim, C., and Parasuk, V. Effects of shape, size, and pyrene doping on electronic properties of graphene nanoflakes. Journal of Molecular Modeling 23 (12) (2017): 355.
- [20] Kim, S., Hwang, S. W., Kim, M.-K., Shin, D. Y., Shin, D. H., Kim, C. O., Yang, S. B., Park, J. H., Hwang, E., Choi, S.-H., Ko, G., Sim, S., Sone, C., Choi, H. J., Bae, S., and Hong, B. H. Anomalous behaviors of visible luminescence from graphene quantum dots: Interplay between size and shape. ACS Nano 6 (9) (2012): 8203-8208.

- [21] Simpson Christopher, D., Brand, J. D., Berresheim Alexander, J., Przybilla, L., Räder Hans, J., and Müllen, K. Synthesis of a giant 222 carbon graphite sheet. Chemistry – A European Journal 8 (6) (2002): 1424-1429.
- [22] Wu, J., Tomović, Ž., Enkelmann, V., and Müllen, K. From branched hydrocarbon propellers to C₃-symmetric graphite disks. The Journal of Organic Chemistry 69 (16) (2004): 5179-5186.
- [23] Bak, S., Kim, D., and Lee, H. Graphene quantum dots and their possible energy applications: A review. Current Applied Physics 16 (9) (2016): 1192-1201.
- [24] Lu, J., Yeo, P. S. E., Gan, C. K., Wu, P., and Loh, K. P. Transforming C₆₀ molecules into graphene quantum dots. Nature Nanotechnology 6 (2011): 247.
- [25] Yan, X., Cui, X., and Li, L.-s. Synthesis of large, stable colloidal graphene quantum dots with tunable size. Journal of the American Chemical Society 132 (17) (2010): 5944-5945.
- [26] Liu, R., Wu, D., Feng, X., and Müllen, K. Bottom-up fabrication of photoluminescent graphene quantum dots with uniform morphology. Journal of the American Chemical Society 133 (39) (2011): 15221-15223.
- [27] Chen, L., Hernandez, Y., Feng, X., and Müllen, K. From nanographene and graphene nanoribbons to graphene sheets: Chemical synthesis. Angewandte Chemie International Edition 51 (31) (2012): 7640-7654.
- [28] Zhang, J., Ong, K. P., and Wu, P. The influence of out-of-plane deformation on the band gap of graphene nanoribbons. The Journal of Physical Chemistry C 114 (29) (2010): 12749-12753.
- [29] Chang, S.-L., Wu, B.-R., Yang, P.-H., and Lin, M.-F. Curvature effects on electronic properties of armchair graphene nanoribbons without passivation. Physical Chemistry Chemical Physics 14 (47) (2012): 16409-16414.
- [30] Yang, Z., Zhang, J., Kintner-Meyer, M. C. W., Lu, X., Choi, D., Lemmon, J. P., and Liu, J. Electrochemical energy storage for green grid. Chemical Reviews 111 (5) (2011): 3577-3613.
- [31] Lu, L., Han, X., Li, J., Hua, J., and Ouyang, M. A review on the key issues for lithium-ion battery management in electric vehicles. Journal of Power Sources 226 (2013): 272-288.

- [32] Tarascon, J. M., and Armand, M. Issues and challenges facing rechargeable lithium batteries. Nature 414 (2001): 359.
- [33] Jansen, A. N., Kahaian, A. J., Kepler, K. D., Nelson, P. A., Amine, K., Dees, D. W., Vissers, D. R., and Thackeray, M. M. Development of a high-power lithium-ion battery. Journal of Power Sources 81-82 (1999): 902-905.
- [34] Scrosati, B. Recent advances in lithium ion battery materials. Electrochimica Acta 45 (15-16) (2000): 2461-2466.
- [35] Scrosati, B. History of lithium batteries. Journal of Solid State Electrochemistry 15 (7) (2011): 1623-1630.
- [36] Whittingham, M. S. Electrical energy storage and intercalation chemistry. Science 192 (4244) (1976): 1126.
- [37] Xiong, Z., Yun, S. Y., and Jin, H.-J. Applications of carbon nanotubes for lithium ion battery anodes. Materials 6 (3) (2013).
- [38] Goriparti, S., Miele, E., De Angelis, F., Di Fabrizio, E., Proietti Zaccaria, R., and Capiglia, C. Review on recent progress of nanostructured anode materials for Li-ion batteries. Journal of Power Sources 257 (2014): 421-443.
- [39] Meng, Y. S., and Arroyo-de Dompablo, M. E. First principles computational materials design for energy storage materials in lithium ion batteries. Energy & Environmental Science 2 (6) (2009): 589-609.
- [40] Thackeray, M. An unexpected conductor. Nature Materials 1 (2002): 81.
- [41] Armand, M., and Touzain, P. Graphite intercalation compounds as cathode materials. Materials Science and Engineering 31 (1977): 319-329.
- [42] Novák, P., Müller, K., Santhanam, K. S. V., and Haas, O. Electrochemically active polymers for rechargeable batteries. Chemical Reviews 97 (1) (1997): 207-282.
- [43] Yamabe, T., Tanaka, K., Ohzeki, K., and Yata, S. Electronic structure of polyacene. A one-dimensional graphite. Solid State Communications 44 (6) (1982): 823-825.
- [44] Kaskhedikar Nitin, A., and Maier, J. Lithium storage in carbon nanostructures. Advanced Materials 21 (25-26) (2009): 2664-2680.
- [45] Guerard, D., and Herold, A. Intercalation of lithium into graphite and other carbons. Carbon 13 (4) (1975): 337-345.

- [46] Yata, S., Hato, Y., Kinoshita, H., Ando, N., Anekawa, A., Hashimoto, T., Yamaguchi, M., Tanaka, K., and Yamabe, T. Characteristics of deeply Li-doped polyacenic semiconductor material and fabrication of a Li secondary battery. Synthetic Metals 73 (3) (1995): 273-277.
- [47] Guo, Y. G., Hu, J. S., and Wan, L. J. Nanostructured materials for electrochemical energy conversion and storage devices. Advanced Materials 20 (15) (2008): 2878-2887.
- [48] Zhu, C., Chao, D., Sun, J., Bacho Ignacio, M., Fan, Z., Ng Chin, F., Xia, X., Huang, H., Zhang, H., Shen Ze, X., Ding, G., and Fan Hong, J. Enhanced lithium storage performance of CuO nanowires by coating of graphene quantum dots. Advanced Materials Interfaces 2 (2) (2014): 1400499.
- [49] Umadevi, D., and Sastry, G. N. Molecular and ionic interaction with graphene nanoflakes: A computational investigation of CO₂, H₂O, Li, Mg, Li⁺, and Mg²⁺ interaction with polycyclic aromatic hydrocarbons. The Journal of Physical Chemistry C 115 (19) (2011): 9656-9667.
- [50] Tachikawa, H. A Direct molecular orbital–molecular dynamics study on the diffusion of the Li ion on a fluorinated graphene surface. The Journal of Physical Chemistry C 112 (27) (2008): 10193-10199.
- [51] Sadlej-Sosnowska, N. Ab initio study of charge transfer between lithium and aromatic hydrocarbons. Can the results be directly transferred to the lithium–graphene interaction? The Journal of Physical Chemistry A 118 (34) (2014): 7044-7051.
- [52] Novák, M., Foroutan-Nejad, C., and Marek, R. Modulating electron sharing in ion- π -receptors via substitution and external electric field: A route toward bond strengthening. Journal of Chemical Theory and Computation 12 (8) (2016): 3788-3795.
- [53] Dirac, P. A. M. Note on exchange phenomena in the Thomas atom. Mathematical Proceedings of the Cambridge Philosophical Society 26 (3) (2008): 376-385.
- [54] Kohn, W., and Sham, L. J. Self-consistent equations including exchange and correlation effects. Physical Review 140 (4A) (1965): A1133-A1138.

- [55] Pople, J. A., and Nesbet, R. K. Self consistent orbitals for radicals. The Journal of Chemical Physics 22 (3) (1954): 571-572.
- [56] Hedin, L., and Lundqvist, B. I. Explicit local exchange-correlation potentials. Journal of Physics C: Solid State Physics 4 (14) (1971): 2064.
- [57] Ceperley, D. M., and Alder, B. J. Ground state of the electron gas by a stochastic method. Physical Review Letters 45 (7) (1980): 566-569.
- [58] 1983. The theory of the inhomogeneous electron gas. New York: Plenum,
- [59] Vosko, S. H., Wilk, L., and Nusair, M. Accurate spin-dependent electron liquid correlation energies for local spin density calculations: a critical analysis. Canadian Journal of Physics 58 (8) (1980): 1200-1211.
- [60] Von Barth, U., and Hedin, L. A local exchange-correlation potential for the spin polarized case. I. Journal of Physics C: Solid State Physics 5 (13) (1972): 1629-1642.
- [61] Janak, J. F., Moruzzi, V. L., and Williams, A. R. Ground-state thermomechanical properties of some cubic elements in the local-density formalism. Physical Review B 12 (4) (1975): 1257-1261.
- [62] Perdew, J. P., and Wang, Y. Accurate and simple analytic representation of the electron-gas correlation energy. Physical Review B 45 (23) (1992): 13244-13249.
- [63] Zhao, Y., and Truhlar, D. G. The M06 suite of density functionals for main group thermochemistry, thermochemical kinetics, noncovalent interactions, excited states, and transition elements: two new functionals and systematic testing of four M06-class functionals and 12 other functionals. Theoretical Chemistry Accounts 120 (1) (2008): 215-241.
- [64] Etacheri, V., Marom, R., Elazari, R., Salitra, G., and Aurbach, D. Challenges in the development of advanced Li-ion batteries: A review. Energy & Environmental Science 4 (9) (2011): 3243-3262.
- [65] Accelrys Materials Studio (Version v 5.5.0.0), Accelrys Inc.: San Diego, USA, 2010.
- [66] Perdew, J. P., Burke, K., and Ernzerhof, M. Generalized gradient approximation made simple. Physical Review Letters 77 (18) (1996): 3865-3868.

- [67] Delley, B. An all-electron numerical method for solving the local density functional for polyatomic molecules. The Journal of Chemical Physics 92 (1) (1990): 508-517.
- [68] Delley, B. Analytic energy derivatives in the numerical local density functional approach. The Journal of Chemical Physics 94 (11) (1991): 7245-7250.
- [69] Casabianca, L. B. Effect of curvature on carbon chemical shielding in extended carbon systems. The Journal of Physical Chemistry A 120 (35) (2016): 7011-7019.
- [70] Frisch, M. J., Trucks, G. W., Schlegel, H. B., Scuseria, G. E., Robb, M. A., Cheeseman, J. R., Scalmani, G., Barone, V., Mennucci, B., Petersson, G. A., Nakatsuji, H., Caricato, M., Li, X., Hratchian, H. P., Izmaylov, A. F., Bloino, J., Zheng, G., Sonnenberg, J. L., Hada, M., Ehara, M., Toyota, K., Fukuda, R., Hasegawa, J., Ishida, M., Nakajima, T., Honda, Y., Kitao, O., Nakai, H., Vreven, T., Montgomery, J. A., Peralta, J. E., Ogliaro, F., Bearpark, M., Heyd, J. J., Brothers, E., Kudin, K. N., Staroverov, V. N., Kobayashi, R., Normand, J., Raghavachari, K., Rendell, A., Burant, J. C., Iyengar, S. S., Tomasi, J., Cossi, M., Rega, N., Millam, J. M., Klene, M., Knox, J. E., Cross, J. B., Bakken, V., Adamo, C., Jaramillo, J., Gomperts, R., Stratmann, R. E., Yazyev, O., Austin, A. J., Cammi, R., Pomelli, C., Ochterski, J. W., Martin, R. L., Morokuma, K., Zakrzewski, V. G., Voth, G. A., Salvador, P., Dannenberg, J. J., Dapprich, S., Daniels, A. D., Farkas, Foresman, J. B., Ortiz, J. V., Cioslowski, J., and Fox, D. J., Gaussian 09, Revision B.01. Wallingford CT, 2009.



Table S1 HOMO-LUMO gaps of CGQDs

CGQDs	Folding axes	Folding angles (degree)	HOMO energies (eV)	LUMO energies (eV)	HOMO-LUMO gaps (eV)
a2x2	1	0	-4.855	-2.488	2.367
		2	-4.853	-2.488	2.365
		4	-4.849	-2.487	2.362
		6	-4.841	-2.485	2.356
		8	-4.830	-2.482	2.348
		10	-4.816	-2.478	2.338
		12	-4.800	-2.474	2.326
		14	-4.780	-2.468	2.312
	16	-4.758	-2.462	2.296	
	2	0	-4.855	-2.488	2.367
		2	-4.852	-2.489	2.363
		4	-4.845	-2.488	2.357
		6	-4.835	-2.488	2.347
		8	-4.822	-2.489	2.333
		10	-4.803	-2.49	2.313
		12	-4.781	-2.492	2.289
		14	-4.753	-2.494	2.259
	16	-4.723	-2.498	2.225	
	3	0	-4.855	-2.488	2.367
		2	-4.853	-2.485	2.368
		4	-4.849	-2.476	2.373
		6	-4.842	-2.461	2.381
		8	-4.832	-2.439	2.393
		10	-4.82	-2.413	2.407
		12	-4.808	-2.383	2.425
		14	-4.794	-2.348	2.446
	16	-4.776	-2.306	2.47	
	4	0	-4.855	-2.488	2.367
		2	-4.853	-2.488	2.365
		4	-4.85	-2.485	2.365
		6	-4.843	-2.48	2.363
		8	-4.834	-2.473	2.361
10		-4.822	-2.465	2.357	
12		-4.808	-2.455	2.353	
14		-4.791	-2.442	2.349	
16	-4.771	-2.429	2.342		
a3x3	1	0	-4.299	-3.179	1.120
		2	-4.298	-3.178	1.120
		4	-4.296	-3.178	1.118
		6	-4.293	-3.176	1.117
		8	-4.288	-3.175	1.113

CGQDs	Folding axes	Folding angles (degree)	HOMO energies (eV)	LUMO energies (eV)	HOMO-LUMO gaps (eV)	
		10	-4.282	-3.173	1.109	
		12	-4.274	-3.169	1.105	
		14	-4.266	-3.166	1.100	
		16	-4.257	-3.163	1.094	
	2	0	-4.299	-3.179	1.120	
		2	-4.297	-3.178	1.119	
		4	-4.292	-3.176	1.116	
		6	-4.284	-3.174	1.110	
		8	-4.273	-3.171	1.102	
		10	-4.261	-3.169	1.092	
		12	-4.246	-3.166	1.080	
		14	-4.227	-3.163	1.064	
		16	-4.206	-3.161	1.045	
		3	0	-4.299	-3.179	1.120
			2	-4.296	-3.174	1.122
			4	-4.290	-3.163	1.127
	6		-4.281	-3.147	1.134	
	8		-4.268	-3.121	1.147	
	10		-4.253	-3.092	1.161	
	12		-4.237	-3.059	1.178	
	14		-4.214	-3.015	1.199	
	4	0	-4.299	-3.179	1.120	
		2	-4.298	-3.177	1.121	
		4	-4.293	-3.172	1.121	
		6	-4.285	-3.165	1.120	
		8	-4.274	-3.154	1.120	
		10	-4.260	-3.140	1.120	
		12	-4.243	-3.123	1.120	
		14	-4.225	-3.105	1.120	
	a4x4	1	0	-4.054	-3.530	0.524
			2	-4.054	-3.530	0.524
			4	-4.054	-3.530	0.524
6			-4.054	-3.530	0.524	
8			-4.054	-3.530	0.524	
10			-4.054	-3.530	0.524	
12			-4.054	-3.530	0.524	
14			-4.055	-3.531	0.524	
16			-4.056	-3.532	0.524	
2		0	-4.054	-3.530	0.524	
		2	-4.052	-3.528	0.524	
		4	-4.048	-3.526	0.522	

CGQDs	Folding axes	Folding angles (degree)	HOMO energies (eV)	LUMO energies (eV)	HOMO-LUMO gaps (eV)	
		6	-4.043	-3.523	0.520	
		8	-4.037	-3.522	0.515	
		10	-4.026	-3.516	0.510	
		12	-4.013	-3.509	0.504	
		14	-4.005	-3.508	0.497	
		16	-3.995	-3.507	0.488	
	3	0	-4.054	-3.530	0.524	
		2	-4.051	-3.526	0.525	
		4	-4.043	-3.515	0.528	
		6	-4.032	-3.498	0.534	
		8	-4.016	-3.474	0.542	
		10	-3.999	-3.446	0.553	
		12	-3.978	-3.413	0.565	
		14	-3.955	-3.373	0.582	
		16	-3.934	-3.333	0.601	
		4	0	-4.054	-3.53	0.524
			2	-4.052	-3.529	0.523
			4	-4.047	-3.523	0.524
	6		-4.038	-3.514	0.524	
	8		-4.026	-3.502	0.524	
	10		-4.012	-3.487	0.525	
	12		-3.994	-3.469	0.525	
	14		-3.973	-3.448	0.525	
	a5x5	1	0	-3.949	-3.710	0.239
			2	-3.950	-3.710	0.240
			4	-3.951	-3.711	0.240
			6	-3.954	-3.713	0.241
			8	-3.957	-3.715	0.242
10			-3.961	-3.718	0.243	
12			-3.966	-3.721	0.245	
14			-3.974	-3.727	0.247	
16			-3.983	-3.734	0.249	
2			0	-3.949	-3.710	0.239
			2	-3.947	-3.708	0.239
			4	-3.944	-3.706	0.238
		6	-3.942	-3.704	0.238	
		8	-3.934	-3.698	0.236	
		10	-3.93	-3.696	0.234	
		12	-3.927	-3.696	0.231	
		14	-3.916	-3.688	0.228	
3		0	-3.949	-3.710	0.239	

CGQDs	Folding axes	Folding angles (degree)	HOMO energies (eV)	LUMO energies (eV)	HOMO-LUMO gaps (eV)
		2	-3.945	-3.704	0.241
		4	-3.937	-3.695	0.242
		6	-3.925	-3.679	0.246
		8	-3.907	-3.656	0.251
		10	-3.889	-3.631	0.258
		12	-3.868	-3.601	0.267
		14	-3.845	-3.568	0.277
		16	-3.845	-3.538	0.307
	4	0	-3.949	-3.710	0.239
		2	-3.947	-3.708	0.239
		4	-3.942	-3.702	0.240
		6	-3.932	-3.692	0.240
		8	-3.920	-3.680	0.240
		10	-3.904	-3.664	0.240
		12	-3.886	-3.645	0.241
		14	-3.866	-3.625	0.241
		16	-3.844	-3.602	0.242
		a6x6	1	0	-3.909
2	-3.909			-3.803	0.106
4	-3.912			-3.805	0.107
6	-3.916			-3.808	0.108
8	-3.921			-3.812	0.109
10	-3.929			-3.819	0.110
12	-3.938			-3.827	0.111
14	-3.951			-3.837	0.114
16	-3.966			-3.850	0.116
2	0		-3.909	-3.803	0.106
	2		-3.906	-3.800	0.106
	4		-3.904	-3.799	0.105
	6		-3.902	-3.797	0.105
	8		-3.900	-3.794	0.106
	10		-3.898	-3.793	0.105
	12		-3.891	-3.788	0.103
	14		-3.892	-3.790	0.102
	16		-3.894	-3.794	0.100
3	0		-3.909	-3.803	0.106
	2		-3.903	-3.797	0.106
	4		-3.896	-3.788	0.108
	6		-3.882	-3.772	0.110
	8		-3.864	-3.752	0.112
	10		-3.847	-3.73	0.117
	12		-3.830	-3.708	0.122
	14		-3.834	-3.671	0.163

CGQDs	Folding axes	Folding angles (degree)	HOMO energies (eV)	LUMO energies (eV)	HOMO-LUMO gaps (eV)
	4	16	-	-	-
		0	-3.909	-3.803	0.106
		2	-3.907	-3.801	0.106
		4	-3.901	-3.794	0.107
		6	-3.891	-3.785	0.106
		8	-3.879	-3.772	0.107
		10	-3.864	-3.757	0.107
		12	-3.846	-3.739	0.107
		14	-3.826	-3.719	0.107
b2x2	1	0	-5.075	-2.320	2.755
		2	-5.074	-2.320	2.754
		4	-5.067	-2.320	2.747
		6	-5.056	-2.319	2.737
		8	-5.042	-2.318	2.724
		10	-5.023	-2.317	2.706
		12	-5.000	-2.316	2.684
		14	-4.974	-2.315	2.659
		16	-4.945	-2.316	2.629
	2	0	-5.075	-2.320	2.755
		2	-5.071	-2.320	2.751
		4	-5.061	-2.322	2.739
		6	-5.043	-2.325	2.718
		8	-5.019	-2.329	2.690
		10	-4.989	-2.336	2.653
		12	-4.954	-2.345	2.609
		14	-4.911	-2.355	2.556
		16	-4.864	-2.368	2.496
b3x3	1	0	-4.672	-2.881	1.791
		2	-4.671	-2.881	1.790
		4	-4.665	-2.879	1.786
		6	-4.655	-2.875	1.780
		8	-4.641	-2.870	1.771
		10	-4.625	-2.865	1.760
		12	-4.605	-2.858	1.747
		14	-4.583	-2.852	1.731
		16	-4.559	-2.847	1.712
	2	0	-4.672	-2.881	1.791
		2	-4.668	-2.880	1.788
		4	-4.657	-2.881	1.776
		6	-4.642	-2.883	1.759
		8	-4.616	-2.883	1.733
		10	-4.590	-2.887	1.703

CGQDs	Folding axes	Folding angles (degree)	HOMO energies (eV)	LUMO energies (eV)	HOMO-LUMO gaps (eV)
		12	-4.559	-2.895	1.664
		14	-4.517	-2.899	1.618
		16	-4.474	-2.909	1.565
b4x4	1	0	-4.457	-3.215	1.242
		2	-4.455	-3.214	1.241
		4	-4.450	-3.211	1.239
		6	-4.441	-3.207	1.234
		8	-4.431	-3.202	1.229
		10	-4.418	-3.196	1.222
		12	-4.403	-3.189	1.214
		14	-4.387	-3.183	1.204
		16	-4.369	-3.177	1.192
	2	0	-4.457	-3.215	1.242
		2	-4.452	-3.213	1.239
		4	-4.443	-3.214	1.229
		6	-4.427	-3.213	1.214
		8	-4.407	-3.214	1.193
		10	-4.385	-3.219	1.166
		12	-4.357	-3.225	1.132
		14	-4.326	-3.232	1.094
		16	-4.297	-3.248	1.049
b5x5	1	0	-4.320	-3.436	0.884
		2	-4.319	-3.435	0.884
		4	-4.314	-3.432	0.882
		6	-4.308	-3.428	0.880
		8	-4.300	-3.423	0.877
		10	-4.290	-3.418	0.872
		12	-4.280	-3.414	0.866
		14	-4.273	-3.412	0.861
		16	-4.268	-3.414	0.854
	2	0	-4.320	-3.436	0.884
		2	-4.314	-3.433	0.881
		4	-4.308	-3.434	0.874
		6	-4.295	-3.433	0.862
		8	-4.278	-3.435	0.843
		10	-4.262	-3.442	0.820
		12	-4.243	-3.451	0.792
		14	-4.227	-3.468	0.759
		16	-4.189	-3.551	0.638
b6x6	1	0	-4.227	-3.591	0.636
		2	-4.225	-3.589	0.636
		4	-4.221	-3.586	0.635
		6	-4.217	-3.583	0.634

CGQDs	Folding axes	Folding angles (degree)	HOMO energies (eV)	LUMO energies (eV)	HOMO-LUMO gaps (eV)
		8	-4.211	-3.579	0.632
		10	-4.205	-3.577	0.628
		12	-4.203	-3.577	0.626
		14	-4.214	-3.588	0.626
		16	-	-	-
	2	0	-4.227	-3.591	0.636
		2	-4.221	-3.587	0.634
		4	-4.214	-3.587	0.627
		6	-4.205	-3.588	0.617
		8	-4.193	-3.591	0.602
		10	-4.185	-3.602	0.583
		12	-4.182	-3.622	0.560
		14	-4.080	-3.768	0.312
		16	-	-	-

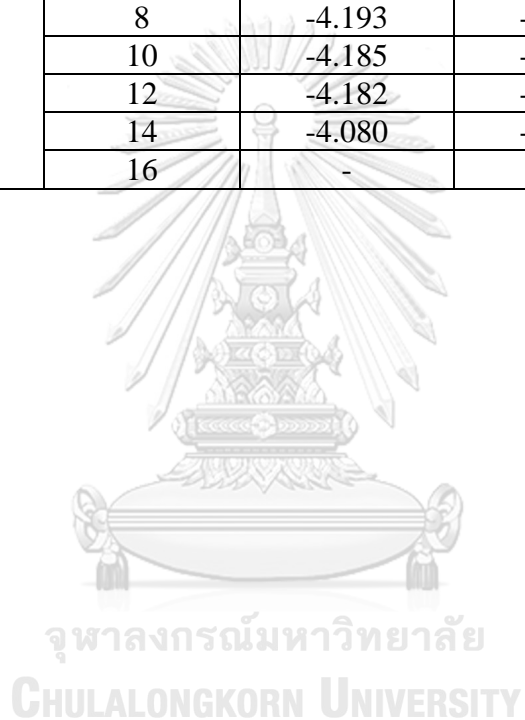


Table S2 Charges of lithium ions of GQDs-2Li⁺ complexes

GQDs	Patterns	Charges of Li ⁺ (atomic unit)					
		GQD (q=-1)		GQD (q=0)		GQD (q=1)	
		1 st Li ⁺	2 nd Li ⁺	1 st Li ⁺	2 nd Li ⁺	1 st Li ⁺	2 nd Li ⁺
C24	1	0.204	0.205	0.526	0.523	0.789	0.789
	2	0.244	0.216	0.524	0.524	NC	NC
	3	0.398	0.398	0.526	0.526	0.794	0.793
	4	0.407	0.407	0.525	0.524	0.789	0.789
C54	1	NC	NC	0.504	0.504	0.565	0.571
	2	NC	NC	0.500	0.550	0.582	0.603
	3	0.467	0.468	0.542	0.543	0.568	0.568
	4	0.475	0.475	0.547	0.547	0.617	0.616
	5	0.190	0.222	0.502	0.500	0.659	0.555
	6	0.405	0.405	0.498	0.499	0.575	0.579
	7	0.417	0.440	0.500	0.503	0.563	0.564
	8	0.427	0.427	0.501	0.501	0.567	0.569
	9	0.428	0.443	0.502	0.505	0.575	0.571
	10	0.428	0.427	0.503	0.501	0.576	0.576
	11	NC	NC	0.491	0.538	0.711	0.595
	12	0.392	0.475	0.488	0.544	0.579	0.597
	13	0.411	0.489	0.498	0.550	0.574	0.601
	14	0.417	0.495	0.501	0.549	0.582	0.604
	15	0.403	0.485	0.492	0.536	0.602	0.600

*NC = No converged result



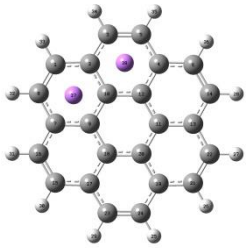
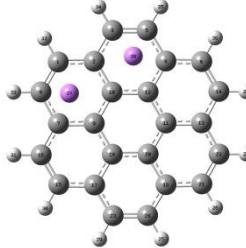
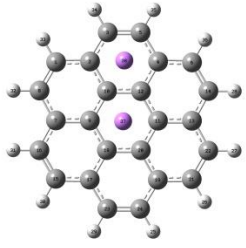
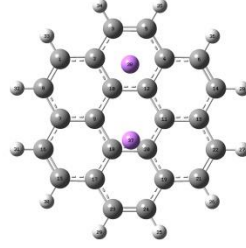
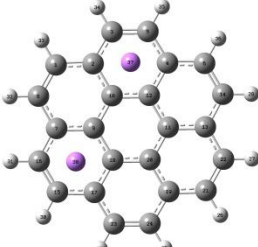
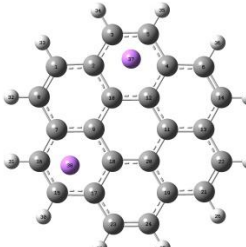
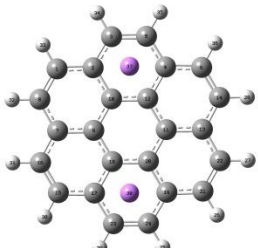
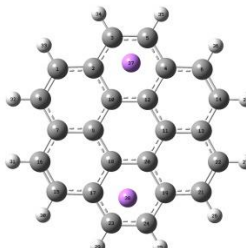
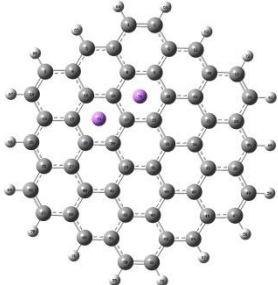
Table S3 Average charges of GQDs and Li⁺ of GQDs-2Li⁺ complexes

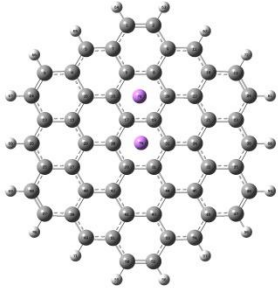
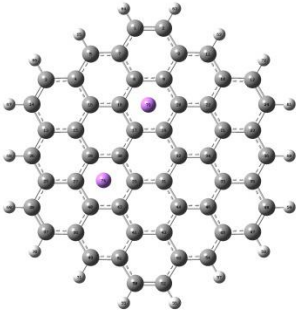
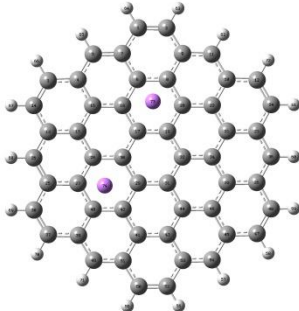
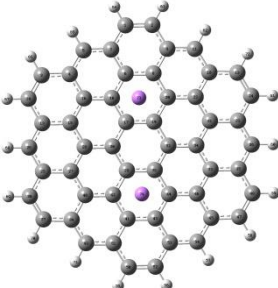
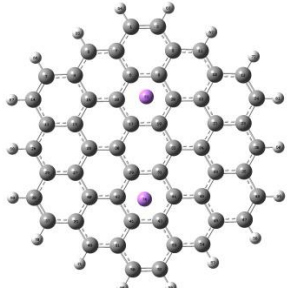
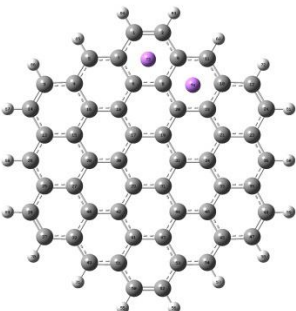
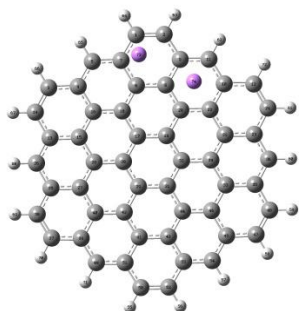
GQDs	Patterns	Average charges of GQDs			Average charges of Li ⁺		
		GQDs ⁻	GQDs	GQDs ⁺	GQDs ⁻	GQDs	GQDs ⁺
C24	1	0.0164	0.0264	0.0395	0.2045	0.5242	0.7893
	2	0.0150	0.0264	NC	0.2303	0.5242	NC
	3	0.0057	0.0264	0.0392	0.3981	0.5257	0.7936
	4	0.0052	0.0264	0.0395	0.4072	0.5243	0.7892
C54	1	NC	0.0108	0.0225	NC	0.5039	0.5681
	2	NC	0.0103	0.0219	NC	0.5251	0.5927
	3	-0.0017	0.0097	0.0226	0.4677	0.5426	0.5681
	4	-0.0019	0.0096	0.0212	0.4754	0.5467	0.6161
	5	0.0054	0.0106	0.0213	0.2058	0.5012	0.6071
	6	-0.0002	0.0107	0.0221	0.4048	0.4981	0.5771
	7	-0.0006	0.0108	0.0226	0.4283	0.5012	0.5638
	8	-0.0005	0.0109	0.0226	0.4269	0.5010	0.5682
	9	-0.0008	0.0109	0.0225	0.4355	0.5033	0.5732
	10	-0.0005	0.0109	0.0224	0.4274	0.5019	0.5763
	11	NC	0.0105	0.0203	NC	0.5144	0.6529
	12	-0.0008	0.0104	0.0220	0.4337	0.5164	0.5879
	13	-0.0012	0.0102	0.0220	0.4500	0.5242	0.5872
	14	-0.0013	0.0103	0.0219	0.4560	0.5250	0.5929
	15	-0.0010	0.0106	0.0217	0.4436	0.5140	0.6011

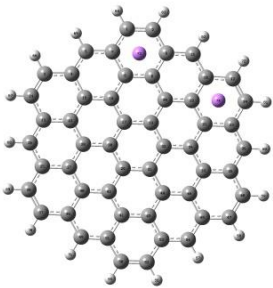
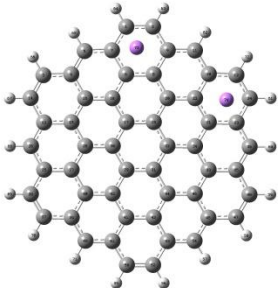
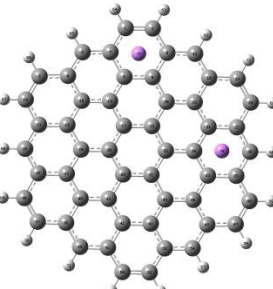
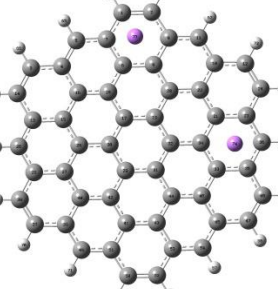
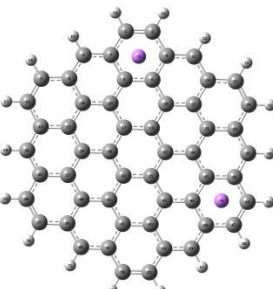
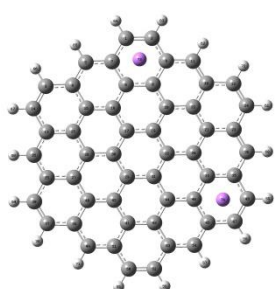
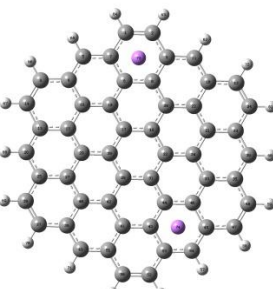
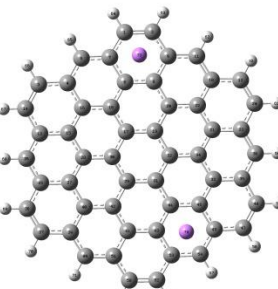
*NC = No converged result

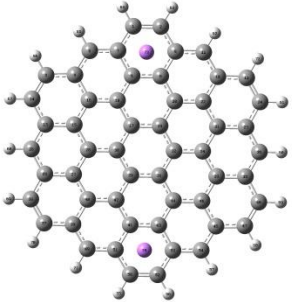
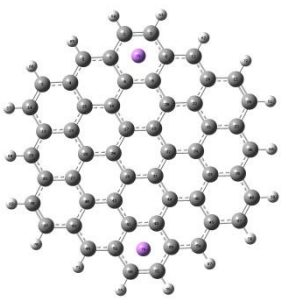
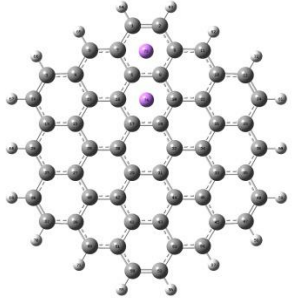
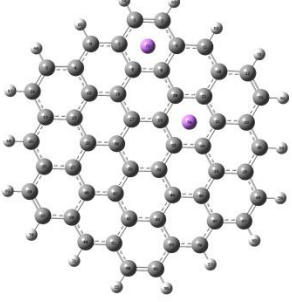
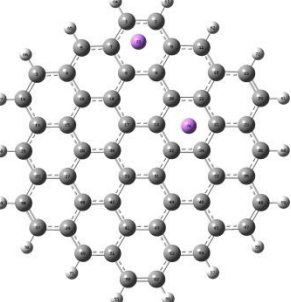
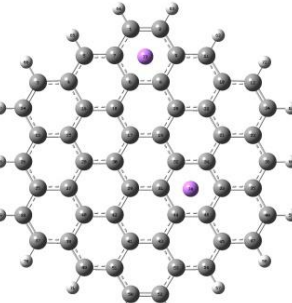
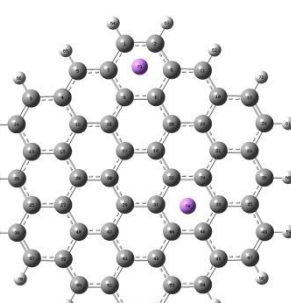


Table S4 Positions of two lithium ion on negative charged GQD

GQDs	Patterns	Positions of 2Li^+	
		Before optimization	After optimization
$\text{C}_{24}\text{H}_{12}$	1		
	2		
	3		
	4		
$\text{C}_{54}\text{H}_{18}$	1		No converged result

GQDs	Patterns	Positions of 2Li ⁺	
		Before optimization	After optimization
	2		No converged result
	3		
	4		
	5		

GQDs	Patterns	Positions of 2Li^+	
		Before optimization	After optimization
	6		
	7		
	8		
	9		

GQDs	Patterns	Positions of 2Li^+	
		Before optimization	After optimization
	10		
	11		No converged result
	12		
	13		

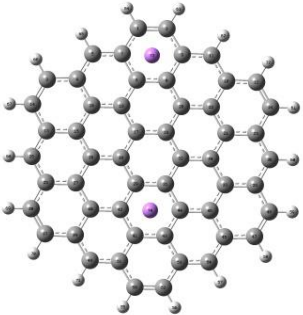
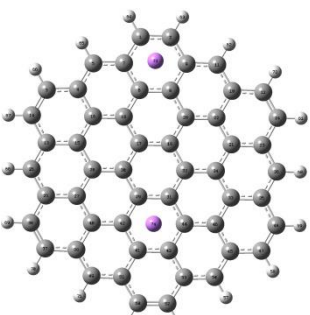
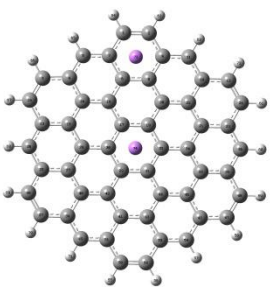
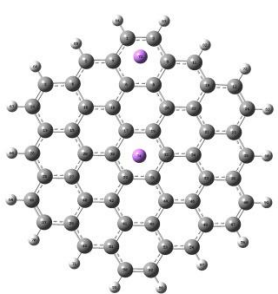
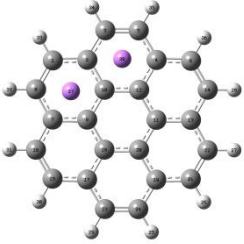
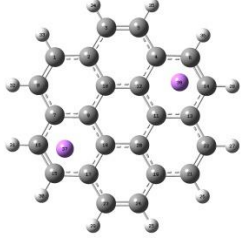
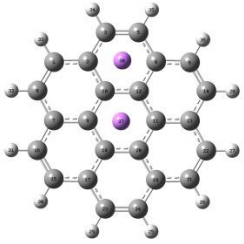
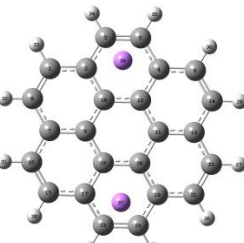
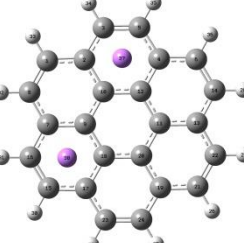
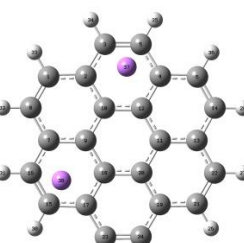
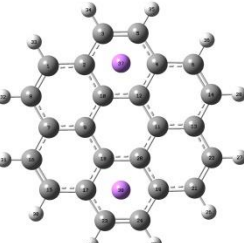
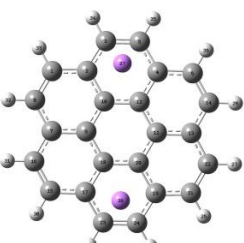
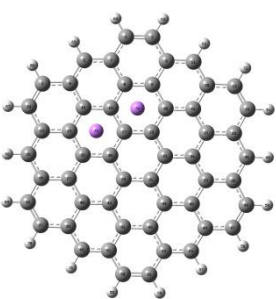
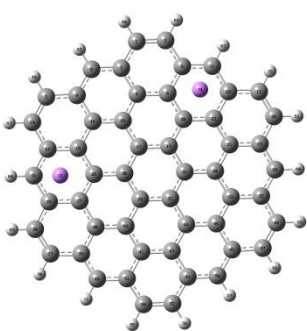
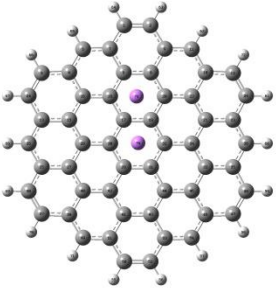
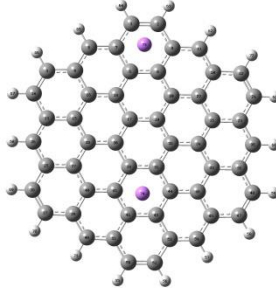
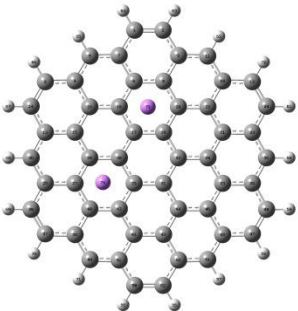
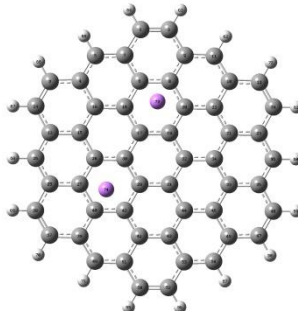
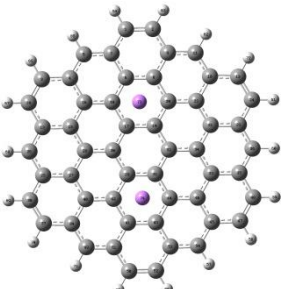
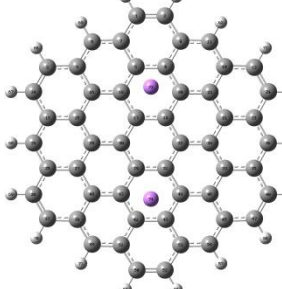
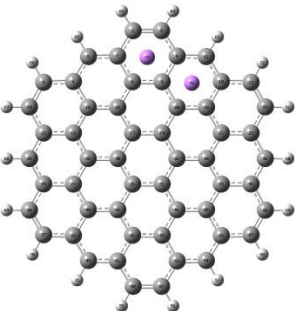
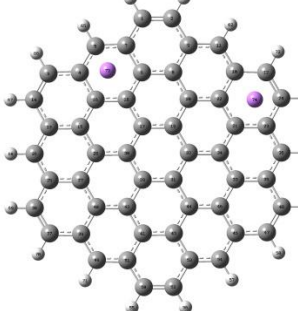
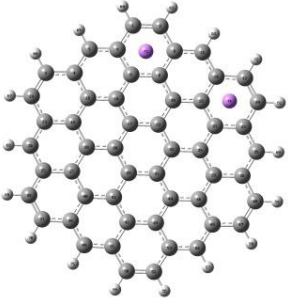
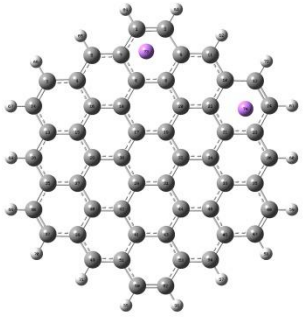
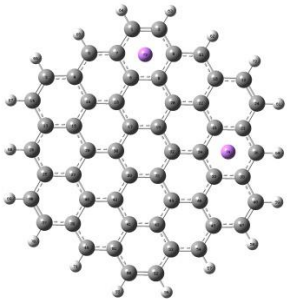
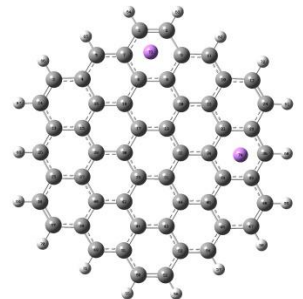
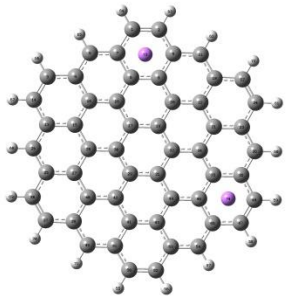
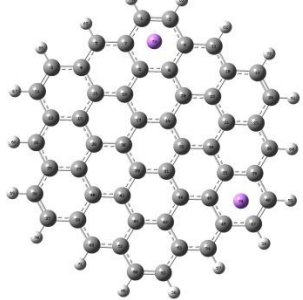
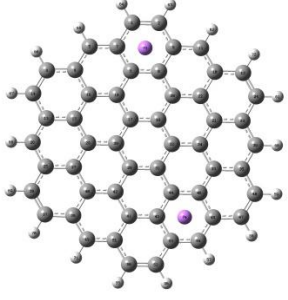
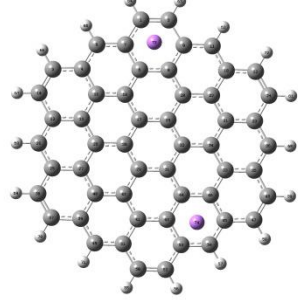
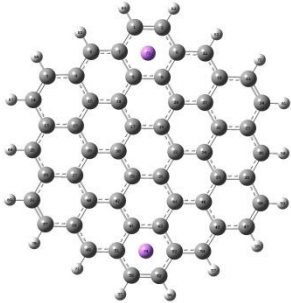
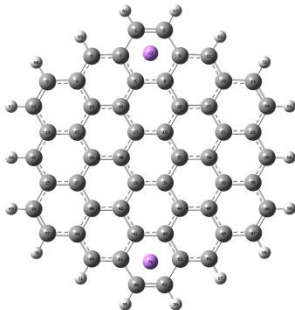
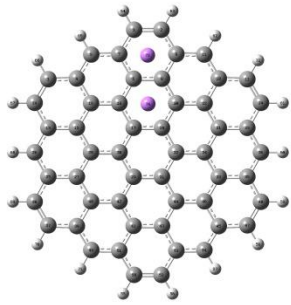
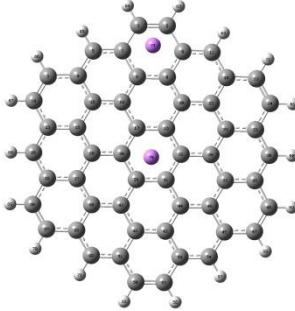
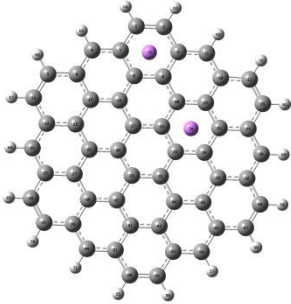
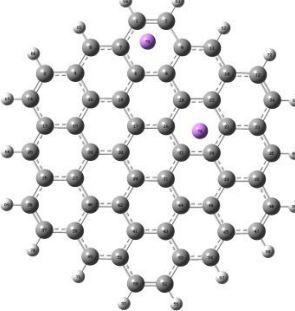
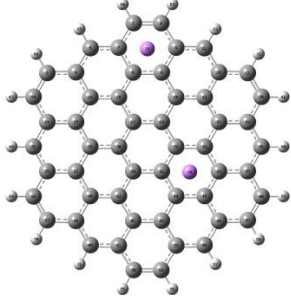
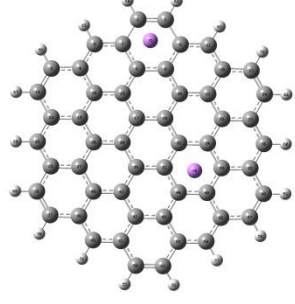
GQDs	Patterns	Positions of 2Li^+	
		Before optimization	After optimization
	14		
	15		

Table S5 Positions of two lithium ion on neutral GQD

GQDs	Patterns	Positions of 2Li^+	
		Before optimization	After optimization
$\text{C}_{24}\text{H}_{12}$	1		
	2		
	3		
	4		
$\text{C}_{54}\text{H}_{18}$	1		

GQDs	Patterns	Positions of 2Li^+	
		Before optimization	After optimization
	2		
	3		
	4		
	5		

GQDs	Patterns	Positions of 2Li^+	
		Before optimization	After optimization
	6		
	7		
	8		
	9		

GQDs	Patterns	Positions of 2Li^+	
		Before optimization	After optimization
	10		
	11		
	12		
	13		

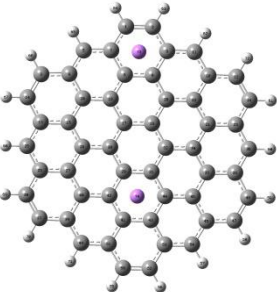
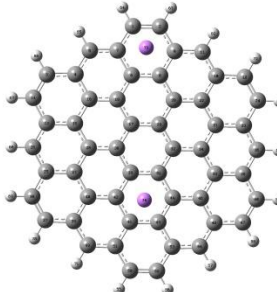
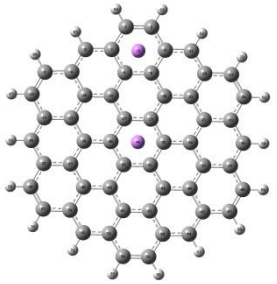
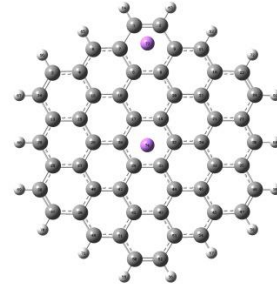
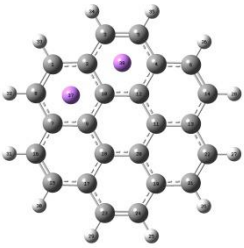
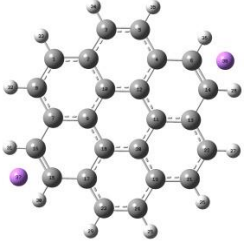
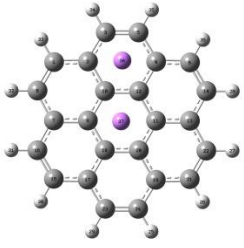
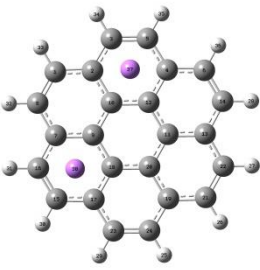
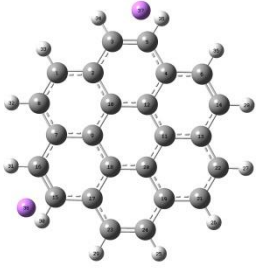
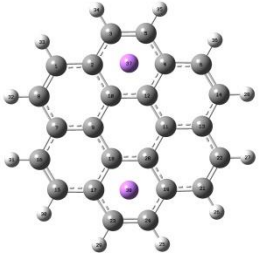
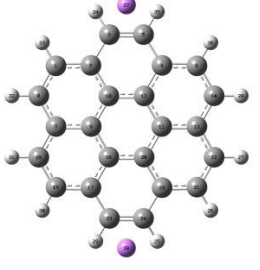
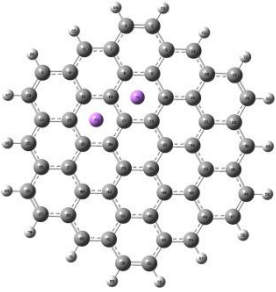
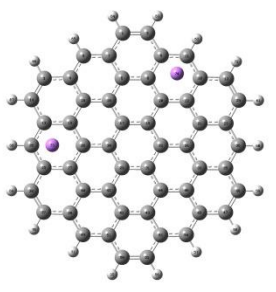
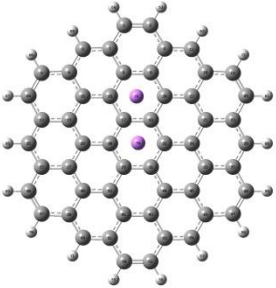
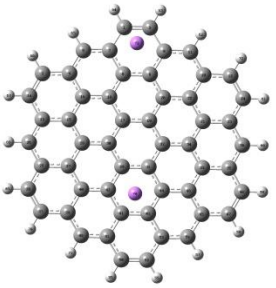
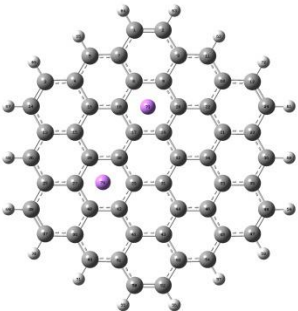
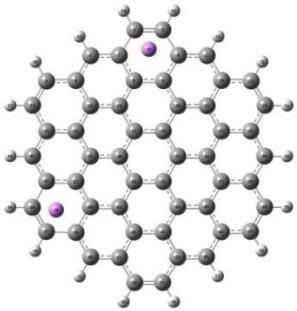
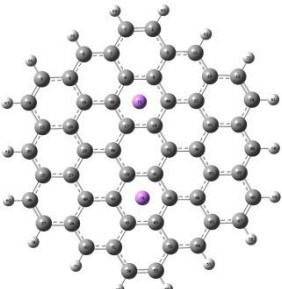
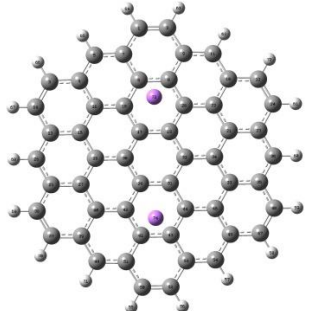
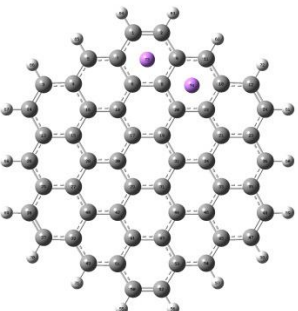
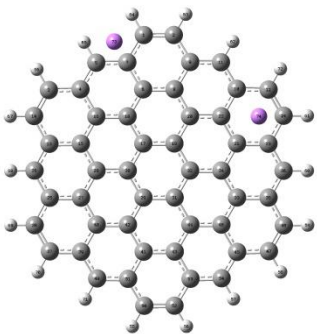
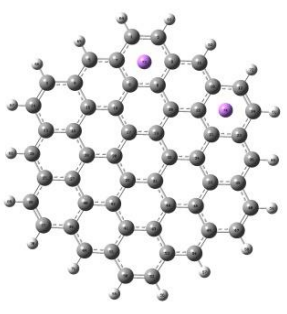
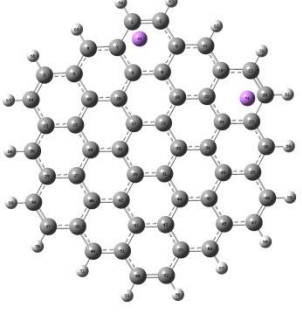
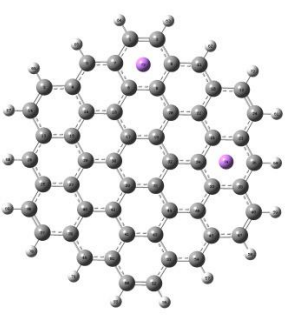
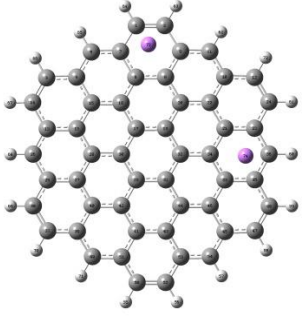
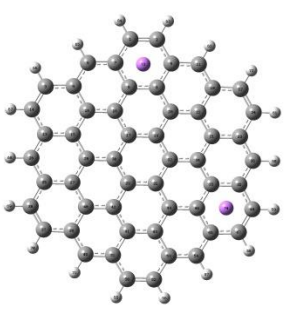
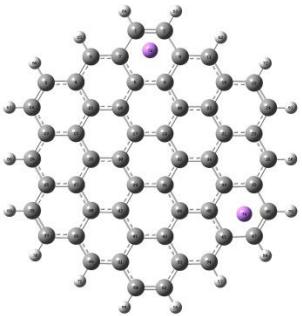
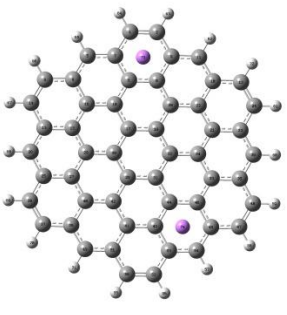
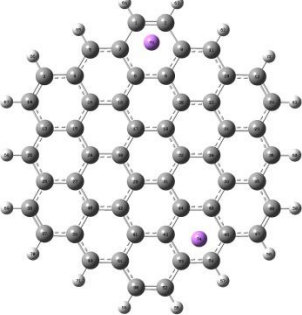
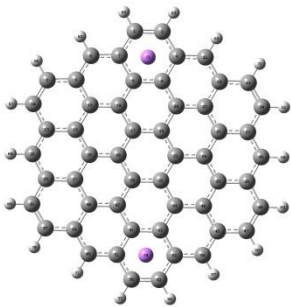
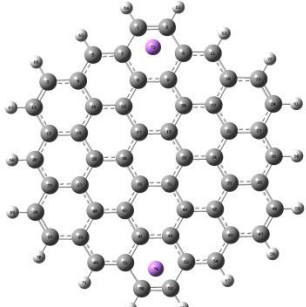
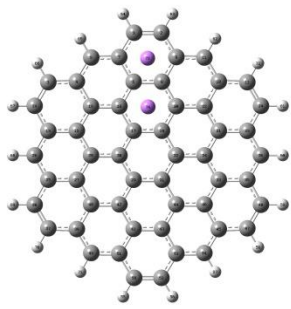
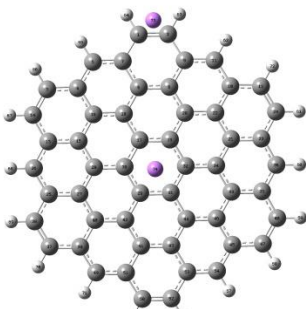
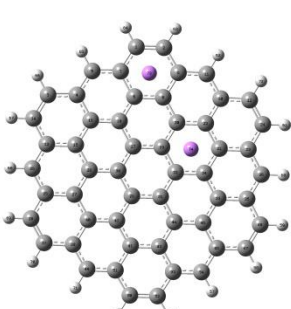
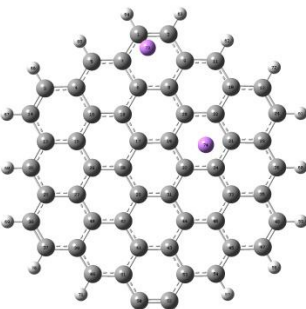
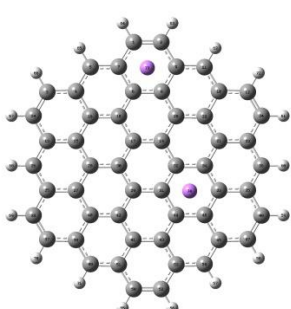
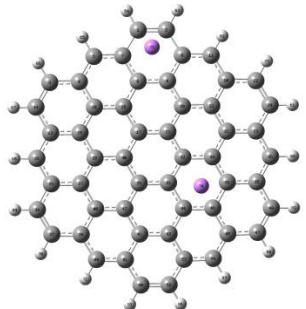
GQDs	Patterns	Positions of 2Li^+	
		Before optimization	After optimization
	14		
	15		

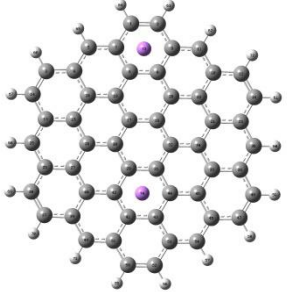
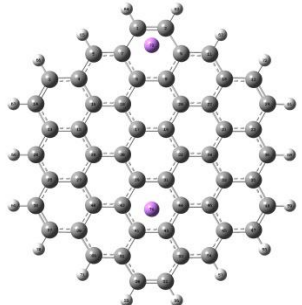
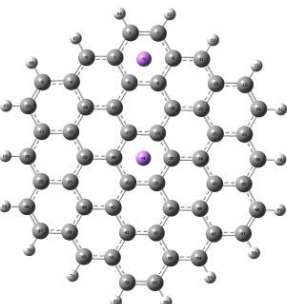
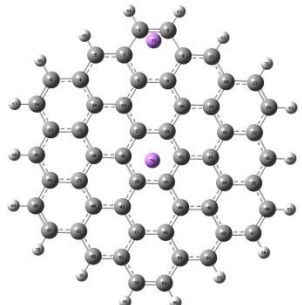
Table S6 Positions of two lithium ion on positive charged GQD

GQDs	Patterns	Positions of 2Li^+	
		Before optimization	After optimization
$\text{C}_{24}\text{H}_{12}$	1		
	2		No converged result
	3		
	4		
$\text{C}_{54}\text{H}_{18}$	1		

GQDs	Patterns	Positions of 2Li^+	
		Before optimization	After optimization
	2		
	3		
	4		
	5		

GQDs	Patterns	Positions of 2Li^+	
		Before optimization	After optimization
	6		
	7		
	8		
	9		

GQDs	Patterns	Positions of 2Li^+	
		Before optimization	After optimization
	10		
	11		
	12		
	13		

GQDs	Patterns	Positions of 2Li^+	
		Before optimization	After optimization
	14		
	15		

VITA

Personal Data:

Name: Naruwan Pattarapongdilok

Mobile Phone: 08-6386-3223

Email: olinpoo@gmail.com, olinpoo@hotmail.com

Education:

2017 - 2018 Grad. Dip. (Teaching Profession), Bansomdejchaopraya Rajabhat University

2014 Certificate in Enhancing 21st Century Pedagogical Content Knowledge and Skills for Secondary Science Teachers, SEAMEO RECSAM, Penang, MALAYSIA

2008 - 2010 M.Sc. (Chemistry), Chulalongkorn University

2004 – 2008 B.Sc. (Chemistry), Chulalongkorn University

Scholarship and Awards:

2015-2018 - Full scholarship from Bansomdejchaopraya Rajabhat University

2012-2015 - Full scholarship from Center of Innovative Nanotechnology (CIN), Chulalongkorn University

2010-2011 - Rachadapisek Sompoch Endowment Fund, Chulalongkorn University

2008-2010 - Full scholarship from National Center of Excellence for Petroleum, Petrochemicals and Advanced Materials (NCE-PPAM)

2008 - Research grant from Chemistry-CU Research Experience Undergraduates (Chem-CU REU)

- Award for best manner and best activist honored by department of chemistry, Faculty of Science, Chulalongkorn University for academic year 2007

2007 - Award for best manner of department of chemistry honored by faculty of science, Chulalongkorn University for academic year 2006

2006 - First runner-up of The Invention and Innovator Project, Faculty of Science, Chulalongkorn University

2004 - Full scholarship from Science Achievement Scholarship of Thailand